Extracellular ATP is a signalling molecule in bacteria

Sophie Tronnet[1,2,3], Vikash Pandey[1,2,3], Miriam Lloret-Berrocal[1,2,3], Mario Pérez-del-Pozo[1,2,3], Niklas Söderholm[1,4], Carlos Hernández-Ortego[1,2,3], Oliver Billker[1,2,3], Anders Nordström[5,6] and Andrea Puhar[1,2,3,7]

[1]The Laboratory for Molecular Infection Medicine Sweden (MIMS), 901 87 Umeå, Sweden

[2]Umeå Centre for Microbial Research (UCMR), 901 87 Umeå, Sweden

[3]Department of Molecular Biology, Umeå University, 901 87 Umeå, Sweden

[4]Department of Chemistry, Umeå University, 901 87 Umeå, Sweden

[5]Umeå Plant Science Centre, 901 87 Umeå, Sweden

[6]Swedish Metabolomics Centre, 907 36 Umeå, Sweden

[7]Wellcome-Wolfson Institute for Experimental Medicine, School of Medicine, Dentistry and Biomedical Sciences, Queen's University Belfast, BT9 7BL Belfast, United Kingdom

Abstract

In animals and plants extracellular ATP (eATP) functions as signalling molecule and regulates the immune response. During inflammation intestinal bacteria are exposed to elevated eATP originating from the mucosa. Whether bacteria respond to eATP is unclear. Here we show that non-pathogenic *Escherichia coli* responds to eATP at physiologically relevant concentrations by modifying its transcriptional and metabolic landscape. The use of a promoter library showed that the response to eATP is time-, dose- and medium-dependent. Genes related to lipid, amino acid, or vitamin metabolism were regulated. Metabolomics showed that eATP triggers enrichment of molecules with bioactive properties on the host or bacteria. Combined genome-scale modelling highlighted the global metabolic modifications. Moreover, eATP altered the sensitivity to antibiotics and antimicrobial peptides. Finally, in pathogens eATP controls the expression of virulence and fitness factors. Our results indicate that eATP is a signalling molecule in prokaryotes which globally regulates physiology, antimicrobial resistance, and virulence.

Introduction

Extracellular ATP (eATP) has emerged as a key signalling molecule in lower and higher eukaryotes, including protozoa, animals, plants, and fungi (Li *et al*, 2021; Medina-Castellanos *et al*, 2014; Medina-Castellanos *et al*, 2018; Pham *et al*, 2020; Tanaka *et al*, 2014; Verkhratsky & Burnstock, 2014). In animals and plants eATP regulates physiological responses (Tanaka *et al.*, 2014; Verkhratsky & Burnstock, 2014). Importantly, eATP controls damage, stress or inflammatory responses in protozoa, animals, plants and fungi upon tissue injury or alteration (Bours *et al*, 2006; Idzko Ferrari & Eltzschig, 2014; Medina-Castellanos *et al.*, 2014; Medina-Castellanos *et al.*, 2018; Pham *et al.*, 2020; Tanaka *et al.*, 2014; Verkhratsky & Burnstock, 2014). In contrast, the existence of purinergic signalling in the earlier forms of life, Bacteria and Archaea, remains largely unexplored (Verkhratsky & Burnstock, 2014).

Whether bacteria can respond to eATP is unclear. Only a handful of studies addressed the effect of eATP on bacteria at the phenotypic level. In *Streptomyces* exogenous ATP promoted differentiation, possibly via cytosolic ATP-consuming enzymes (Li *et al*, 2016; Li *et al*, 2008; Meng *et al*, 2011). Other studies investigated the role of added

ATP in biofilms and/or growth in several organisms, partially with opposing results. Effects on biofilms were linked to release of biofilm-composing DNA upon eATP-induced lysis (Xi & Wu, 2010), inhibition of twitching motility by reducing surface-assembled Type IV pili via eATP hydrolysis (Nolan *et al*, 2015), chelation of biofilm-composing cations by eATP (Ding & Tan, 2016), or not further dissected (Baeza & Mercade, 2021). Effects on growth were not explained (Abbasian *et al*, 2019; Li *et al*, 2011; Malo *et al*, 2014; Xi & Wu, 2010), except for eATP-dependent chelation of the nutrient iron in one instance (Tatano *et al*, 2015). However, whether eATP acts as signalling molecule remains unsolved. Finally, ATP supplementation increased survival of non-growing bacteria (Mempin *et al*, 2013).

Until recently, a contribution of eATP to host-microbe interactions was not appreciated. However, eATP is present in the nano- to micromolar range in culture supernatants (Atarashi *et al*, 2008) or homogenates (Chiaranunt *et al*, 2023) of murine faeces and many isolated bacteria (Abbasian *et al.*, 2019; Baeza & Mercade, 2021; Chiaranunt *et al.*, 2023; Ding Quah & Tan, 2016; Hironaka *et al*, 2013; Ihssen *et al*, 2021; Ivanova *et al*, 2006; Iwase *et al*, 2010; Mempin *et al.*, 2013; Nolan *et al.*, 2015; Qiu *et al*, 2019), during osmotic shock (Berrier *et al*, 1992), treatment with antimicrobial peptides (Alvarez *et al*, 2017; Valat *et al*, 2003) or antibiotics (Abbasian *et al.*, 2019; Ihssen *et al.*, 2021; Nilsson, 1978; Proietti *et al*, 2019; Yu Lomakina & Ugarova, 2022). During homeostasis, eATP is found in the gut lumen at low concentration (Kusu *et al*, 2013; Malo *et al.*, 2014; Patel, 2014; Perruzza *et al*, 2017; Proietti *et al.*, 2019; Puhar *et al*, 2013; Scott *et al*, 2021; Tani *et al*, 2021). Importantly, intestinal eATP increases during bacterial, viral, or parasitic infection and protist colonisation. Indeed, enteropathogenic bacteria trigger connexin-dependent secretion of ATP from the intestinal epithelium, *via* activation of the mechanosensor PIEZO1, as an early alert response, which induces potent gut inflammation (Puhar *et al.*, 2013; Tadala *et al*, 2022). Rotavirus also initiates epithelial purinergic signalling (Chang-Graham *et al*, 2020). During Shiga toxin-producing enterohaemorrhagic *Escherichia coli* (Arvidsson *et al*, 2022) or *Citrobacter rodentium* infection (Chiaranunt *et al.*, 2023) and *Tritrichomonas musculis* colonisation (Chiaranunt *et al*, 2022) eATP is present in faeces. Helminths induce ATP release in the gut (Chen *et al*, 2022). Further, intestinal eATP rises during experimental inflammatory bowels diseases (IBD) (Di Virgilio Pinton & Falzoni, 2016; Kurashima *et al*, 2012; Scott *et al.*, 2021; Wan *et al*, 2016) and after irradiation in graft-versus-host-disease (Wilhelm *et al*, 2010) and small intestinal fibrosis (Takemura *et al*, 2018). Ultimately, any process causing cell damage results in ATP release (Verkhratsky & Burnstock, 2014). Together, this implies that in the gut lumen, during infection and inflammation, commensal and pathogenic microbes are exposed to heightened concentrations of eATP, which may serve as environmental signal.

Here we show that eATP regulates the transcriptional and metabolic landscapes of non-pathogenic *E. coli* at physiologically relevant concentrations. The response to eATP presents the characteristic of bacterial transcriptional and metabolic networks, and result in production of bioactive compounds and altered susceptibility to antimicrobials. We further show that several gut pathogens and pathobionts respond to eATP by regulating expression of virulence or fitness factors. Together, our results indicate that eATP is a signalling molecule that modifies the physiology of harmless and pathogenic bacteria, allowing them to adapt to a changing environment.

Results

eATP triggers a robust transcriptional response in non-pathogenic *E. coli*

To investigate the ability of bacteria to sense and respond to eATP, we tested whether eATP induces a transcriptional response using a plasmid-based fluorescent reporter library in non-pathogenic *E. coli* K-12 MG1655 (Zaslaver *et al*, 2006). This collection can unravel the dynamic activity of approximately 2000 promoters (75% of *E. coli* promoters), allowing accurate quantification of gene expression induction or repression seen as GFP fluorescence normalised to the number of bacteria.

We screened this library for a response to eATP in rich (LB) and minimal medium (M9) upon treatment with 1 mM ATP for 3 h (Fig EV1A). Addition of ATP led to up- or down-regulation of promoters in both media, with a higher fraction modulated in M9 than in LB (Fig 1A-D, examples in Fig EV1B-G, Table EV1). We identified 291 and 476 modulated promoters in LB and M9, respectively (Fig 1E), with 121 promoters modulated by eATP in both media, of which 46 genes were upregulated and 27 downregulated (Fig 1F, G). These screens were highly reproducible (Fig EV1H), and addition of ATP neither altered bacterial growth (Fig EV1J-L) nor caused changes in pH.

To investigate whether the transcriptional response to eATP in *E. coli* MG1655 is dose- and time-dependent, we selected three reporters that were significantly upregulated by eATP at 3 h in LB and/or M9: P*ybjX*, controlling the expression of a DUF535 domain-containing protein; P*rstA*, controlling the DNA-binding transcriptional regulator of the two-component system RstAB; and P*gadW*, controlling a DNA-binding transcriptional dual regulator. We applied increasing concentrations of eATP and measured the promoter activity in LB (Fig 1H-J) and M9 (Fig 1K-M) over time. This showed that the response to eATP was dose-dependent for all tested promoters in both media after 60 min of stimulation or longer, except for the promoter activity of *gadW*, which never increased with the addition of eATP in M9 (Fig 1L). We confirmed the activity of two upregulated promoters by constructing chromosomal fusions with superfolder GFP. Both endogenous promoters of *gadW* and *cbpA* (which controls the expression of a DnaK co-chaperone) were significantly upregulated (fold change≈2) 5 and 30 min after eATP addition, respectively (Fig EV1M-O).

To understand what the response to eATP in non-pathogenic *E. coli* MG1655 is, we analysed the function of eATP-modulated genes. Several of these genes encode unknown or poorly characterized proteins (Table EV1). KEGG analysis revealed 13 and 15 significantly enriched pathways in LB and M9, respectively, including the metabolism of fatty acids, vitamins, co-factors and proteinogenic amino acids (Fig 2A, b and Table EV1). Quorum sensing, riboflavin and nitrogen metabolism were enriched in both media. In contrast, the metabolism of different types of vitamins, amino acids and fatty acids was predicted in LB and M9. We further analysed the differentially expressed genes (DEGs) using the web-based tool Panther (Mi *et al*, 2013), which functionally classified them into four general gene ontology (GO) categories: biological processes, cellular components, molecular function, and protein class (Fig 2C, Table EV1). The DEGs modulated in LB and M9 upon stimulation with eATP were mainly found in the subcategories: binding, catalytic activity, cellular processes, metabolic process, cellular anatomical entity, and metabolite interconversion enzyme and to a lesser extent, transporter and gene-specific transcriptional regulator, confirming the prediction that eATP impacts bacterial gene regulation and metabolism.

In summary, these results show that the intestinal non-pathogenic bacterium *E. coli* responds to eATP at physiologically relevant concentrations by modifying its transcriptional landscape in a medium-, dose- and time-dependent manner.

eATP triggers a strong metabolic response in non-pathogenic *E. coli*

Our data indicated that the gene expression programmes induced by eATP have a strong impact on bacterial physiology and metabolism. To validate this finding, we assessed the changes in intracellular (pellet) and extracellular (supernatant) metabolites of bacteria grown in LB or M9 upon exposure to eATP by untargeted metabolomics using liquid chromatography–mass spectrometry (LC–MS/MS). We only measured extracellular metabolites in M9 because LB cannot be employed in LC-MS/MS.

In unstimulated *E. coli* MG1655, we detected 57 and 53 intracellular metabolites in LB and M9, respectively, with 51 present in both media. Further, we identified 89 extracellular metabolites, with 61 only present in the supernatant but not the pellets, while 23 metabolites were found in all conditions (Fig 3A and Table EV2). We then compared the metabolome of bacteria stimulated with 1 mM ATP for 3 h with time-matched unstimulated controls. Partial least square-discriminant analysis (PLS-DA) distinguished untreated and eATP-treated *E. coli* (Fig 3B-D), indicating a clear effect of eATP on the metabolome. Univariate analysis of these data revealed that eATP triggers a potent shift in the metabolic landscape (Fig 3E-J, Table EV2), with 5–16% of detected metabolites significantly modulated (≥1.5 FC, $P \leq 0.05$) in response to eATP. The metabolic changes upon ATP addition in M9 were more substantial than in LB with 9/53 and 4/57 significantly modulated metabolites in pellets, respectively (Fig EV2A-D, Table EV2), confirming the medium-dependent effect of eATP we observed in transcriptional assays (Fig 1). We found 11/89 significantly eATP-modulated metabolites in the supernatant (Fig EV2E-F, Table EV2).

Overall, the most recurrently modulated metabolites were intermediates of fatty acid, co-factor, small organic acid, pentose phosphate, vitamin, nucleotide and nucleoside, proteinogenic and non-proteinogenic amino acid biosynthesis, and redox regulation (Fig 3E-J, Table EV2). This is in keeping with the predicted regulation of metabolic pathways based on the eATP-dependent transcriptional changes. To identify the most characteristic metabolites in LB and M9, we calculated VIP scores, ranking the metabolites according to their influence on the separation of the treatment groups (Fig EV2B, D, F). To analyse these differences in depth, we constructed metabolic models (see below). Among the metabolites not integrated in the metabolic model, ophthalmic acid was significantly decreased in LB (Fig 3H, Table EV2). In M9, cAMP and lysine were strongly decreased, while PC-caproyl (a membrane lipid) was upregulated by eATP (Fig 3I, Table EV2). Further, the analysis showed that the upregulated biogenic amine tyramine was the top ranked metabolite in the VIP analysis in the M9 supernatant (Fig 3H, Fig EV2E-F). Of note, allantoin, AMP, threonate and GTP also accumulated in the supernatant.

To test whether the metabolic response to eATP is dose-dependent, alike the transcriptional response, as proof of principle we assessed the changes in intracellular metabolites of *E. coli* MG1655 grown in M9 upon stimulation with 100 μM ATP. This showed that the metabolites in treated bacteria were easily discriminated from the unstimulated control (Fig EV3A) and revealed shifts in the abundance of several compounds from proteinogenic and non-proteinogenic amino acid, fatty acid, small organic acid, pentose phosphate, nucleotide and nucleoside, cell envelope, co-factor metabolism and redox regulation (Fig EV3B-F, Table EV2). Intracellular metabolites in bacteria treated with 100 μM or 1 mM eATP were only partially different (Fig EV3G-H). Two compounds (cAMP and L-lysine – Fig 3I and Fig EV3E, Table EV2) were significantly negatively modulated by eATP at both concentrations, while arginosuccinic acid and L-pipecolate decreased at 100 μM eATP (Fig EV3E). Interestingly, tyramine accumulated in 100 μM eATP-treated bacteria, as observed for

1 mM eATP. These results show that the response to eATP is concentration-dependent at quantitative level (seen as duration and strength of transcriptional induction) and also leads to cells to different metabolic states.
Altogether, our results show that eATP triggers a strong metabolic response in a non-pathogenic bacterium in a medium- and dose-dependent manner.

Comprehensive genome-scale modelling reveals medium-specific differences in *E. coli* metabolic capabilities induced by eATP.

To gain a comprehensive understanding of the key properties of eATP-modulated metabolic networks, we performed genome-scale metabolic modelling by integrating transcriptional and intracellular metabolomic data from *E. coli* MG1655 exposed to 1mM ATP using REMI (Pandey Hadadi & Hatzimanikatis, 2019).
The analysis revealed that in LB 78% (141/181) and in M9 59% (138/233) of the omics-based constraints were consistently integrable with the model (Table EV3), indicating that nutrient-rich medium provides more metabolic flexibility. We performed differential flux analysis and identified 316 and 430 reaction fluxes that were significantly (*P* value <1e-3) modulated for LB and M9, respectively (Table EV3). ATP stimulation enriched the following metabolic subsystems in both LB and M9: valine, leucine and isoleucine metabolism; murein synthesis and recycling; and cell envelope biosynthesis. Glycerophospholipid metabolism was modulated in LB, while in M9 the core metabolism (pentose phosphate pathway and citric acid cycle), non-essential amino acid metabolism (proline and arginine), purine and pyrimidine nucleotide biosynthesis were modulated (Fig 4A-B, Table EV3). These analyses further highlight the medium-specific differences in metabolic capabilities induced by eATP.
To understand the downstream effects of transcriptional, metabolite and reaction perturbations, we calculated the abundance of 68 Biomass Building Blocks (BBBs), which are important indicators of bacterial physiology, with focus on amino acids, lipids and co-factors (Table EV3). eATP caused marked modulation (>1.5-fold) of 6 BBBs in LB and 5 in M9 (Fig 4C). In both LB and M9, the production of L-leucine increased, while L-lysine and KDO(2)-lipid IV(A), an essential component of lipopolysaccharide, were overproduced only in LB. In M9 the production of L-valine and L-isoleucine increased but decreased in LB. Oxidized flavin adenine dinucleotide (FAD) and riboflavin production diminished in M9. These findings indicate that BBBs synthesis, and thereby the chemical nature of bacterial structures such as the cell envelope, is altered by eATP in a medium-dependent manner.
Finally, to obtain a metabolic snapshot of the global changes induced by eATP, we identified subnetworks that contain both significantly modulated reaction fluxes and metabolites or genes (Fig 4D and 5). This very stringent analysis highlights pathways that are consistently altered at many levels. Most reactions were increased upon addition of eATP in both media (seen in iterative quantitative simulations shown in boxes), with a few exceptions: UMPK (see figure legend for abbreviations) and INSH in LB (Fig 5) and GLUPRT in M9 (Fig 5). eATP modulated the nucleotide salvage network in LB and M9, but the extent and pattern of deregulation differed. Purine-nucleoside phosphorylase-dependent reactions (PUNP2, PUNP5 encoded by *b4384*, and PUNP6 encoded by *b2407*) play a vital role in recycling purines. Expression of *b2407* was not altered by eATP in M9, while *b4384* was downregulated in LB (Table EV1). In LB only inosine, UMP, uridine, and few reactions (PUNP5 and INSH) were impacted by eATP. By contrast, in M9 the network showed modular deregulation, with several metabolites (inosine, adenosine, adenine, UMP, uracil) and reactions (PUNP2, PUNP6, DADA, and AMPN) being modulated by eATP. UMP was

upregulated in both media, but produced through UPPRT reaction in M9, whilst through NTPP8, UMPK or URIK1 in LB. Moreover, N-acetyl-glutamate, ADP and oxidized glutathione accumulated in M9 in presence of eATP. While there is no direct interaction between N-acetyl-glutamate and oxidized glutathione, they may influence each other indirectly, as the reaction fluxes of GTHS and ACGS were higher in M9 in presence of eATP. Further, D-ribose-5 phosphate increased, together with directly or indirectly linked reactions associated with nucleotide salvage pathways (AMPN), pentose-phosphate pathway (TKT1), co-factor and prosthetic group biosynthesis (NNAM) as well as purine/pyrimidine biosynthesis (GLUPRT). Of note, ATP addition led to a slight but significant decrease of nicotinamide (vitamin B3), a precursor of the essential redox co-factor nicotinamide adenine dinucleotide (NAD).
These results highlight the potent impact of eATP on whole metabolic pathways the metabolism of non-pathogenic *E. coli*, including on the production of crucial cellular components and of compounds with known bioactive properties on bacteria or the host. Moreover, these findings underscore the importance of considering the cellular context when analysing changes in metabolic networks induced by eATP.

eATP alters antibiotics and antimicrobial peptides susceptibility

During infection, bacteria may be exposed to eATP in conjunction with environmental insults such as antibiotic therapy and antimicrobial peptides from the host. Our results indicate that eATP triggers global physiological changes, some of which modify the cell envelope in non-pathogenic *E. coli*. Therefore, we tested the sensitivity of eATP-pretreated bacteria to selected antibiotics and antimicrobial peptides of diverse origin and various modes of action (Table EV5). Non-pathogenic *E. coli* showed enhanced susceptibility to aztreonam, mecillinam, and gentamicin and reduced susceptibility to ceftazidime and imipenem (Fig 6A). Bacteria treated with eATP showed a marked increased susceptibility to all tested antimicrobial peptides except CAP-18 (Fig 6B-H and Fig EV4A-G). Altogether, eATP alters the sensitivity to antibiotics or antimicrobial peptides.

The ability to respond to eATP is present among clinically relevant bacteria

We explored whether the capacity to respond to eATP by modifying the transcriptional landscape is present in bacteria other than non-pathogenic *E. coli* MG1655. We selected a panel of harmless, pathobiontic or pathogenic Enterobacteriaceae: non-pathogenic *E. coli* BW25113, adherent invasive *E. coli* (AIEC) LF82 (pathobiontic), probiotic *E. coli* Nissle 1917, enteropathogenic *E. coli* (EPEC), enteroinvasive *E. coli* (EIEC), pathogenic *Shigella flexneri* (enteroinvasive), S*almonella enterica* serovar Typhimurium (enteroinvasive) and *Klebsiella pneumoniae*.
We transformed these organisms with transcriptional fluorescent reporter plasmids carrying promoters from *E. coli* MG1655 that were activated by eATP (Fig 1, Fig EV1 and Table EV1). To estimate the chances of *E. coli* MG1655 promoters to function in these bacteria, we performed multiple sequence alignments and sequence identity analyses (Fig EV5A). This revealed a high percentage of identity among all *E. coli* strains and *S. flexneri*, whereas *S*. Typhimurium and *K. pneumoniae* showed lower identity compared to *E. coli* MG1655. All tested Enterobacteriaceae displayed a transcriptional response to eATP in LB and M9 that was within the same range as *E. coli* MG1655, with a few exceptions (Fig 6I, Fig EV5B); P*gadW-gfp* in *E. coli* Nissle 1917 was only activated in M9, while we detected no activation in *S. flexneri* or *S*. Typhimurium. None of the reporters responded to eATP in *K. pneumoniae* grown in

M9. We omitted experiments with *S. flexneri*, EIEC and *S*. Typhimurium in M9 owing to their poor growth.
These results indicate that eATP is a signalling molecule for medically relevant bacteria. While in Enterobacteriaceae the ability to respond to eATP is conserved, the type of response is strain- and species-specific.

The expression of virulence factors is regulated by eATP

We showed that eATP elicits transcriptional responses in pathogenic bacteria, exploiting target genes that are mostly present in both non-pathogenic *E. coli* and the pathogens. To determine whether eATP could also regulate strain-specific virulence genes, we cloned the promoter of selected virulence and fitness factors into the transcriptional reporter plasmid, which we introduced into the bacteria of origin, and monitored promoter activity upon eATP stimulation.
We selected the promoters of *S*. Typhimurium *mgtC*, *hilA*, and *ssrB*. In *Salmonella*, pathogenicity islands 1 and 2 (SPI-1 and SPI-2) have crucial roles in early and later stages of infection, respectively (Lou *et al*, 2019). HilA positively controls the expression of SPI-1 genes (Ellermeier Ellermeier & Slauch, 2005), while the two-component system SsrAB regulates the expression of several SPI-2 operons (Deiwick *et al*, 1999). MgtC aids bacterial survival inside macrophages (Choi *et al*, 2019). Addition of ATP significantly upregulated P*mgtC* and downregulated P*hilA* in a dose-dependent manner (Fig 6J), whilst P*ssrB* was not regulated (Fig EV5C).
E. coli Nissle 1917 contains a *pks* genomic that mediates the synthesis of colibactin, a genotoxin (Nougayrède *et al*, 2006). ClbR is a key transcriptional regulator of the *pks* island (Wallenstein *et al*, 2020). Stimulation with high concentrations of eATP resulted in a decrease of the *clbRA* promoter activity (Fig 6K).
We also tested the promoter of *E. coli* LF82 *qseBC*. This strain was isolated from a mucosal lesion of a Crohn´s disease patient (Darfeuille-Michaud *et al*, 1998). It adheres to and invades enterocytes, and replicates within macrophages. The pathogenicity of LF82 and that of many *E. coli* depends on the quorum-sensing two-component system QseBC (Rooks *et al*, 2017). Upon treatment with eATP, the promoter activity of LF82 *qseBC* significantly decreased at all eATP concentrations except 5 mM (Fig 6L).
Finally, we tested P*ler* and P*grlA* from EPEC E2348/69. EPEC encodes a pathogenicity island, the locus of enterocyte effacement (LEE). LEE is activated by the master regulators Ler and GrlA (Platenkamp & Mellies, 2018). While the activity of P*grlA* strongly diminished in a dose-dependent manner (Fig 6M), P*ler* remained unaltered (Fig EV5D).
Together, these findings indicate that eATP can regulate virulence and fitness in a broad panel of clinically important intestinal bacteria.

Discussion

In lower and higher eukaryotes, eATP is a universal signalling molecule that acts as danger signal (Bours *et al.*, 2006; Tanaka *et al.*, 2014; Verkhratsky & Burnstock, 2014). Whether eATP functions as signalling molecule in prokaryotes has been a longstanding question. Here we show that heightened eATP elicits extensive changes in physiology and virulence by reprogramming transcriptional and metabolic landscapes in a panel of Enterobacteriaceae. In non-pathogenic *E. coli*, this alters the envelope composition and the sensitivity to antibiotics or antimicrobial peptides.
In eukaryotes, danger signals positively and negatively regulate defence mechanisms, ultimately promoting survival. For example, in mammals eATP initiates immunity and

also promotes healing (Bours *et al.*, 2006). But how would the activity of a danger signal manifest in bacteria? The eATP-mediated loss of viability upon exposure to antimicrobial peptides and some antibiotics is difficult to reconcile with the expected protective function of a bacterial danger signal. Rather, this effect points to an additional host defence mechanism, where ATP released by stressed cells directly weakens bacteria, besides inducing inflammation (Puhar *et al.*, 2013). Of note, elevated eATP augments the production of gut antimicrobial peptides during experimental shigellosis (Puhar *et al.*, 2013), setting the conditions to exploit this enhanced sensitivity. Importantly, our data indicate that the potency of antimicrobials may be altered in inflammatory environments, where eATP is abundant. This is of therapeutic concern for the antibiotics showing reduced efficacy in the presence of eATP.

By contrast, up- or downregulation of virulence and fitness factors downstream of eATP seems in line with a function as danger signal to bacteria. The dose-dependency of the response indicates that microbes may utilise eATP as a site- and infection stage-characteristic environmental signal, which provides an additional regulatory layer to finetune species-specific adaptation. Indeed, we speculate that different niches in the gut have distinctive eATP concentrations during inflammation, akin to oxygen tension gradients (Marteyn *et al*, 2010). In healthy tissue the extracellular space is virtually devoid of ATP, while injured cells release up to millimolar ATP from their cytosolic 3-10 mM ATP pool (Bours *et al.*, 2006). Hence, eATP is likely most abundant at its site of release, the mucosa, and gradually diffuses into the gut lumen. Thus, harmless microbes in the lumen might be exposed to lower eATP than pathobionts or pathogens adhering to the epithelium. Invasive bacteria encounter secreted ATP during cellular uptake (Tadala *et al.*, 2022) and peaking ATP after vacuolar escape (Malik-Kale Winfree & Steele-Mortimer, 2012). Accordingly, we generally observed downregulation of early-stage and upregulation of late-stage virulence genes, when eATP is highest. However, a larger number of virulence factors must be tested.

Moreover, eATP is a ubiquitous inflammatory mediator, for example in the airways (Idzko *et al*, 2007). Notably, *K. pneumoniae* is carried in the respiratory and gastrointestinal tracts (Raffelsberger *et al*, 2021). Finally, heightened eATP in dense microbial communities could regulate bacterial adaptation, for instance in survivors of bacteriophage- or antibiotic-induced death (Abbasian *et al.*, 2019; Ihssen *et al.*, 2021; Nilsson, 1978; Proietti *et al.*, 2019; Yu Lomakina & Ugarova, 2022). Altogether, this warrants comprehensive investigation of the impact of eATP on diverse organisms in various environments and its potential role as danger signal in prokaryotes.

In eukaryotes, eATP acts as a signal in the micro- to millimolar range (Bours *et al.*, 2006; Pham *et al.*, 2020; Tanaka *et al.*, 2014; Verkhratsky & Burnstock, 2014). We provide evidence supporting a bacterial response at these eATP levels. As in eukaryotes, we found that eATP modifies bacterial gene expression. In non-pathogenic *E. coli*, eATP triggered only partially overlapping promoter activities in different media. In fact, the output to an external cue is a global function of distinct input components: the cue and the cellular state. The latter strongly depends on the environment (Gianchandani *et al*, 2009), thus giving rise to media-specific responses. Further, the existence of early and late gene expression programmes reflects the hierarchical structure of transcriptional regulatory systems, which are comprised of environmental stimuli at the top and multiple lower levels of transcriptional regulators and target genes (Gianchandani *et al.*, 2009).

Likewise, in different media eATP induced only partially overlapping shifts in compounds of diverse chemical nature and genome-scale metabolic networks. As for

transcriptional states, several regulatory mechanisms influence metabolic fluxes, including reactant concentration (depending on the environment and cellular state), enzyme abundance (depending on gene expression), and enzyme kinetic parameters (Covert & Palsson, 2002; Gerosa & Sauer, 2011), thus explaining medium-specific metabolite changes. Introduction of ATP as a substrate may contribute to the observed changes in intra- and extracellular purines. While eATP is neither transported into *E. coli* (Mempin *et al.*, 2013; Tjaden *et al*, 1998) nor serves to phosphorylate bacterial molecules (Mempin *et al.*, 2013), its components may be internalised after ATP hydrolysis. Indeed, carbon flux mapping in intracellular *S.* Typhimurium showed that ribose and nucleobases partly and fully originate from the host, respectively, rather than from *de novo* synthesis (Mitosch *et al*, 2023). Altogether, our data reveal that the eATP response presents the characteristics of bacterial gene regulatory networks and metabolic fluxes.

Among the metabolites modulated by eATP, we detected intracellular cAMP. This second messenger is produced downstream of environmental signals and regulates carbon metabolism, stress response pathways and virulence (McDonough & Rodriguez, 2011). Further, eATP stimulated the production of metabolic intermediates or end products with described bioactive properties on microorganisms or the host (Culp & Goodman, 2023; Krautkramer Fan & Bäckhed, 2021), for example antioxidants and the neurotransmitter tyramine (a complete list is provided in Table EV2). We found modulation of vitamins at the transcriptional level, but not by metabolomic analysis, possibly due to the extraction protocol (Krautkramer Fan & Bäckhed, 2021). Cross-feeding of vitamins is common among intestinal bacteria (Culp & Goodman, 2023). Likewise, quorum sensing was transcriptionally upregulated, but we didn't detect autoinducers. Altogether, this points to the activation of intracellular signalling pathways in bacteria downstream of sensing eATP, which culminate in the production of compounds potentially regulating intra- and inter-kingdom cell-to-cell communication.

The mechanism by which bacteria sense and respond to eATP remains to be elucidated. A molecular understanding of bacterial eATP signalling is key to predict which species encode the ability to utilise eATP as environmental cue and to assess, under well-controlled conditions, the role of eATP-mediated host-bacteria interactions in complex systems such as the gut. Our discovery of eATP-dependent transcriptional and metabolic regulation of bacteria, together with its molecular dissection, may open unfathomed opportunities for the prevention and treatment of infection and inflammation.

In conclusion, we show that eATP rewires physiology, antimicrobial sensitivity, and virulence in medically important intestinal bacteria. Thus, eATP emerges as a potent signalling molecule in prokaryotes.

Acknowledgements

A.P. acknowledges institutional support from MIMS (Vetenskapsrådet grant 2021-06602) and Umeå University Medical Faculty, Knut and Alice Wallenberg Foundation grant KAW 2015.0225, Umeå University Bioteknikmedel FS 2.1.6-1862.17 and Insamlingsstiftelse FS 2.1.6-452-20, Vetenskapsrådet project grant VR-MH 2022-00778, Carl Kempe Foundation grant SMK-1859, and institutional support from Queen's University Belfast. S.T. acknowledges Svenska Sällskapet för Medicinsk Forskning (SSMF) for postdoctoral grant P19-0098. We thank David A. Cisneros (Queen's University Belfast) for critical reading.

449 **Conflict of Interests**
450 The authors declare that they have no conflict of interest.
451
452 **Contributions**
453 Conceptualization: S.T. and A.P.
454 Data curation: S.T.
455 Formal analysis: S.T., V.P., M.L.B., M.P.P., C.H.O., A.N.
456 Funding acquisition: S.T. and A.P.
457 Investigation: S.T., M.L.B., M.P.P., C.H.O., A.N.
458 Methodology: V.P.
459 Project administration: A.P.
460 Resources: O.B.
461 Software: S.T., V.P. and N.S.
462 Supervision: S.T. and A.P.
463 Validation: S.T. and A.P.
464 Visualization: S.T.
465 Writing – Original Draft: S.T., V.P. and A.P.
466 Writing – Reviewing and editing S.T., V.P., M.L.B., M.P.P., N.S., C.H.O., O.B., A.N.,
467 A.P.
468
469 **Material and methods**
470
471 **Reagents**
472 Unless stated otherwise, all chemicals, antibiotics and primers were purchased from
473 Sigma-Aldrich. Restriction and cloning enzymes were obtained from New England
474 Biolabs (NEB). Unless stated otherwise, plasticware for bacterial culture was
475 purchased from Techno Plastic Products (TPP) and Greiner. ATP sodium salt solution
476 100 mM was obtained from ThermoFisher (reference R0441). Antimicrobial peptides
477 were purchased from Eurogentec. Antibiotic MIC strips were obtained from Liofilchem.
478
479 **Bacterial strains and culture conditions**
480 The bacterial strains used in this study are listed in Table EV4. Bacteria were
481 preserved as glycerol stocks at -80°C. Bacterial cultures in rich medium were
482 performed in Luria Broth (LB) 1X medium (yeast 5 g/l; tryptone 10 g/l; NaCl 5 g/l).
483 Bacterial cultures in minimal medium were performed in M9 (M9 salts 1X; $CaCl_2$ 0,1
484 mM; $MgSO_4$ 2 mM; glucose 0,5 %). Kanamycin (25 µg/ml) was added to the medium
485 when needed. If not specified, overnight bacterial cultures were grown at 37°C in the
486 medium of choice, subcultured 1:100, and grown at 37°C in a shaking incubator at 150
487 RPM until mid-exponential phase (OD_{600nm} = 0.3-0.5).
488
489 **Screen for genome-wide promoter activity in *E. coli* MG1655 using a**
490 **transcriptional reporter library**
491 The library of reporter strains, each carrying a low-copy plasmid (pUA66-*mut2GFP*)
492 with a promoter of interest controlling fast-folding GFP (GFPmut2), was previously
493 described (Zaslaver *et al.*, 2006) and purchased from Dharmacon. The library was
494 replicated to accommodate positive and negative controls to create a working library,
495 resulting in punctual changes in sample position with respect to the original library.
496 The disposition of samples is provided in Table EV1. Reporter strains were inoculated
497 in 96-well plates from frozen stocks and grown overnight in the medium of choice with
498 kanamycin at 37°C in a shaking incubator. Overnight cultures were diluted 1:100 into

150 µl of fresh medium containing kanamycin in black 96-well plates with an optical flat bottom (Greiner). The cultures were incubated at 37°C in a shaking incubator at 150 RPM. When the mid-exponential phase was reached, 50 µl of medium containing 4 mM ATP was added to each well to obtain a final concentration of 1 mM ATP in each well. In each plate, a strain carrying a promoterless plasmid was included as a background control. Optical density (OD_{600nm}) and fluorescence intensity (excitation: 485 nm; emission: 535 nm) were measured in an Infinite M200 or a Spark plate reader (Tecan) just before (t=0 min) and after ATP addition (time=5 min) and then measured at intervals of 60 min for 240 min, with incubation at 37°C in a shaking incubator at 150 RPM between measurements. The expression levels were calculated by subtracting the background fluorescence (promoterless strain) and by dividing the intensity of fluorescence by the corresponding OD_{600nm}. The reproducibility of the screening was verified by plotting the normalised fluorescence of a random plate measured on day 1 against the values on day 2. Promoters showing a final fluorescence value lower than 100 in both ATP-treated and control samples were considered as not expressed. The ratio of the fluorescent signal produced by eATP-treated bacteria and untreated control bacteria was calculated. The screen was performed twice in LB and in M9, hence statistical analysis was not performed.

Construction of chromosomal reporter fusions

Reporter fusions were constructed using Red recombination as previously described (Gerlach *et al*, 2007). The kanamycin resistance cassette was amplified from pKD4 with ST1_aph_KpnI_F and ST2_aph_XhoI_R, cloned into a KpnI/XhoI digested pBluescript plasmid and named pBluescript-kan (See Table EV4). The same procedure was performed with the PCR-amplified msfGFP Addgene plasmid # 29750 and subcloned into EcoRI/HindIII-digested pBluescript-kan. This PCR fragment contained a ribosome binding site upstream of *msfGFP.* The final plasmid construct was verified by sequencing. PCR amplification of msfGFP-Kan was performed using the newly cloned plasmid using ST5_cbpA_sfGFP_aph_F and ST6_cbpA_sfGFP_aph_R as templates. The PCR product was digested with DpnI and transformed into *E. coli* MG1566 carrying pKD56. Colonies were selected on plates containing 50 µg/mL kanamycin and verified by sequencing. The kanamycin resistance gene was removed by FLP-mediated recombination (Datsenko & Wanner, 2000; Gerlach *et al.*, 2007).

Measurement of promoter activity upon ATP addition at small scale

To determine promoter activities at different concentrations of added ATP, in *E. coli* MG1655 carrying chromosomal fusion reporters and in all strains other than *E. coli* MG1655 from the transcriptional reporter library (Figure 6), the experimental protocol was adjusted to the smaller scale compared to the screening setup. The reporter strains used in these experiments were directly inoculated in 3 ml of appropriate medium with kanamycin for 16 h at 37°C and 150 RPM. The cultures were then diluted to obtain a final OD_{600nm}=0,01 using the medium of choice at a final volume of 150 µl per well in black 96-well plates with an optical flat bottom (Greiner) and, as previously described, grown until mid-exponential phase. After incubation, 50 µl of medium containing the appropriate ATP concentration was added to each well to obtain 100 µM, 500 µM, 1 mM, 2 mM or 5 mM in the final volume (200 µl). The optical density and fluorescence were measured, and data were analysed as described above (screening section). Experiments were performed in at least 3 biological replicates with 2 or 3 technical replicates.

549
550 **Panther analysis and KEGG pathway analysis**
551 To investigate the biological functions and gene ontology of differentially expressed
552 genes (DEGs, FC>1,5) upon exposure to 1 mM ATP, DAVID Bioinformatics
553 Resources version 6.8 (Huang da Sherman & Lempicki, 2009) and the PANTHER
554 classification system version 17.0 (Thomas *et al*, 2003) were used to functionally
555 annotate and classify genes. The reference list for the GO enrichment analysis
556 contained 1,807 modulated genes of the transcriptional reporter library (Zaslaver *et*
557 *al.*, 2006).
558
559 **Sample preparation for untargeted metabolomics**
560 *E. coli* MG1655 was grown overnight at 37°C in the medium of choice. The cultures
561 were diluted to obtain a final OD_{600nm}=0,01 in 20 mL of appropriate medium and
562 incubated until mid-exponential phase at 37°C under agitation. The subculture was
563 divided into 5 ml samples for each condition. ATP was added (100 µM or 1 mM), and
564 the tubes were incubated at 37°C under agitation for 3 h. The time-matched control
565 samples were supplemented with an equal volume of distilled water. Samples of 2 ml
566 were collected in 2 ml microtubes (Sarstedt, ref 72.690.001) 180 min after the addition
567 of the compounds and centrifuged at 13000 x *g* for 2 min. The supernatant of M9-
568 cultured bacteria was filtered (pore size: 0,22 µm, diameter: 13 mm, syringe-driven,
569 Millex) and collected in a sample tube. The bacterial pellets were washed 3 times with
570 ice-cold PBS keeping cells on ice between centrifugations. Both the supernatant and
571 the pellet were stored at -20°C until analysis. At least 3 biological replicates were
572 prepared for each condition.
573
574 **Metabolite extraction for untargeted metabolomics**
575 Bacterial pellets were solubilized using 200 µl 90:10 MeOH:H_2O and were stored at -
576 80°C or kept on dry ice. Acid-washed glass beads of 425-600 µm diameter (Sigma
577 Aldrich) were added to samples kept on dry ice to constitute 50% v/v of the 90:10
578 MeOH:H_2O cell suspension, and cells were disrupted by shaking at 30 Hz for 2 min
579 (Mixer Mill MM400, Retsch) using prechilled (4°C) holding blocks. Samples were
580 centrifuged at 4°C and 14000 x *g* for 10 min, followed by transfer of the supernatant
581 into an LC–MS vial (Chromacol, 03-FISV, Thermo Fisher, MA, USA). Samples were
582 evaporated in a centrifugal evaporator (Speed Vac, Savant) at room temperature until
583 dry and stored at -80°C, and reconstituted with 20 µl 60:40 MeOH:H_2O prior to LC-MS
584 analysis.
585
586 **LC–MS analysis of metabolites**
587 Five microliters were injected into a 1290 Infinity II LC UHPLC system (Agilent, CA,
588 USA) connected to either a 6550 Series or 6540 Series Q-TOF mass spectrometer
589 (Agilent, CA, USA) with a Jet Stream electrospray ionization (ESI) source (Agilent, CA,
590 USA). Data were collected in positive and negative ionization mode with ESI settings:
591 gas temperature 150°C, drying gas flow 16 l/min, nebulizer pressure 35 psi, sheath
592 gas temperature 350°C, sheath gas flow 11 l/min, Vcap 4000 V, nozzle voltage 300
593 V, Fragmentor voltage 380 V, Skimmer1 45 V and OctapoleRFPeak 750 V.
594 Metabolites were separated using reversed-phase chromatography using an
595 ACQUITY UPLC HSS T3 column with C18 chemistry, 1.8 µM particle size, and 100 Å
596 pore size of 50 mm length and 2.1 mm inner diameter (Waters, MA, USA). For
597 reversed-phase chromatography, elution solvents were (A) H_2O, 0.1% formic acid and
598 (B) 75:25 acetonitrile:isopropanol, 0.1% formic acid. For separation, the following

599 linear gradient was used (flow rate 0.5 ml/min): min 0: 0.1% B, min 2: 10% B, min 7:
600 99% B, min 9: 99% B, min 9.3: 0.1% B, min 10.8: 0.1% B. Column re-equilibration
601 occurred from 9.8 to 10.7 min with an increase in flow rate to 0.8 ml/min.
602
603 **Metabolite identification and relative quantification**
604 Raw data was processed using Agilent Mass Hunter Profinder software and the
605 metabolites were identified with an inhouse retention time accurate mass library
606 constructed using synthetic standards on the same analytical setup. A retention time
607 window of 0.5 minutes and a mass accurace tolerance of 5 ppm was employed. A
608 statistics-based analysis of the metabolites was performed using MetaboAnalyst 5.0,
609 a web-based metabolomics processing tool (Chong Wishart & Xia, 2019). The peak
610 area for each metabolite was uploaded to the MetaboAnalyst program and normalised
611 using log transformed and autoscaling features (mean-centred and divided by the
612 standard deviation of each variable). If values were missing, an estimate was
613 performed using K-nearest neighbours' imputation. A one-way ANOVA using Tukey's
614 honestly significant difference test was used to determine significant features. Partial
615 least squares-discriminant analysis (PLS-DA) was used to examine differences
616 between the groups. Metabolites with a *P* value<0,05 and fold change (FC)>1,5 were
617 considered significantly modulated. The normalised peak area of each differential
618 metabolite was used to construct the bar plots. Heatmaps were constructed to provide
619 an overview of the metabolome changes, and PLS-DA was used to show the 25 most
620 important features. VIP (Variable Importance in Projection) values (≥1.0) and
621 Student's *t* test (*P* value <0.05) were combined to identify the differential metabolites.
622 The VIP score is a weighted sum of squares of the PLS loadings. The weights are
623 based on the amount of explained Y-variance in each dimension. Metabolites with
624 high VIP are more important in providing class separation, while those with small VIP
625 provide less contribution.
626
627 **Susceptibility tests to antibiotics and antimicrobial peptides**
628 *E. coli* MG1655 was grown overnight at 37°C in LB. The cultures were diluted to obtain
629 a final OD_{600nm}=0,01 in 10 mL of medium and incubated until mid-exponential phase
630 at 37°C under agitation. The subculture was divided into 3 ml samples for each
631 condition. ATP (1 mM) or mock were added, and the tubes were incubated at 37°C
632 under agitation for 3 h.
633 Resistance to various antibiotics was determined on agar using MIC Test Strips
634 (Liofilchem). Exponential cultures were adjusted to OD_{600nm}=0,1 in LB and
635 homogeneously spread onto an LB agar plate containing or not 1mM ATP. The strip
636 was applied once the plates had fully dried. Plates were incubated over night at 37°C
637 and the MIC at which the no-growth halo was observed was determined visually.
638 Susceptibility to antimicrobial peptides (Eurogentech) was tested by adjusting the
639 OD_{600nm}=0,04 in LB, 50 µl of culture were distributed into a 96-well plate (TPP),
640 followed by 150 µl containing serially diluted antimicrobial peptides together with
641 vehicle or 1 mM ATP. Plates were maintained at 37°C with 3 mm linear agitation in a
642 Spark multimode plate reader (Tecan) and the OD_{600nm} was acquired every 10 min.
643 Seven antimicrobial peptides were used: indolicidin, apidaecin IB, CAP-18, cecropin,
644 melittin, protegrin-1, C18G (see also Table EV4). The antimicrobial peptide stock
645 solutions were prepared beforehand in sterile water and kept at −80°C until usage,
646 except for protegrin-1 and C18G, which were prepared in 0,01% acetic acid before
647 freezing. Experiments were performed in biological triplicates with 2 or 3 technical
648 replicates.

649
650 **Cloning of promoter regions into pUA66-*GFPmut2***
651 The high-fidelity polymerase Phusion was used for all PCRs. All plasmid constructs
652 were verified by sequencing (Eurofins). Plasmids and oligos are listed in Table EV4.
653 Promoter regions (positions with respect to start ATG) of *mgtC* (-480 to 113), *grlA* (-
654 89 to 143), *hilA* (-700 to 457), *clbRA* (-537 to 156), *qseBC* (-480 to 109), *ler* (-407 to
655 108) and *ssrAB* (-431 to 112) were PCR amplified with primers containing either *XhoI*
656 or *BamHI* restriction sites, using DNA extracted from the relevant organisms with the
657 Wizard® genomic purification kit (Promega) according to manufacturer´s instructions.
658 The purified PCR products were XhoI/BamHI digested. The plasmid pUA66-mut2GFP
659 was XhoI/BamHI digested and purified in a 1% agarose gel run at 100 V for 40 min in
660 TAE buffer, followed by isolation with the GeneJet gel extraction kit (ThermoScientific).
661 The digested PCR products and backbone plasmid were ligated using T4 DNA ligase
662 (Thermo Fisher Scientific). The mixture was transformed into $CaCl_2$-competent *E. coli*
663 DH5α. Transformants were selected on LB agar plates containing 25 µg/ml
664 kanamycin. A few colonies were picked and screened by colony PCR using primers
665 (Table EV4) designed for the upstream and downstream regions of the two restriction
666 sites. Verified recombinant plasmids were purified and transformed into the organisms
667 of promoter origin by electroporation.
668
669 **Generation of a phylogenetic tree and percentage identity calculation**
670 A phylogenetic tree of the employed strains based on NCBI taxonomy was generated
671 with PhyloT (https://phylot.biobyte.de/index.cgi). The visualization of the tree was
672 achieved using iTOL (https://itol.embl.de/) (Letunic & Bork, 2021). Taxonomy numbers
673 used for the tree are shown in Table EV4. To calculate the percentage identity of
674 *gadW*, *ybjX*, *slyB* and *rstA* between the different strains, the nucleotide sequences
675 were downloaded for every strain and aligned using MUSCLE v5
676 (https://www.ebi.ac.uk/Tools/msa/muscle/). The identity of each sequence compared
677 to the selected reference sequence (*E. coli* MG1655) was calculated using The
678 Sequence Manipulation Suite (https://www.bioinformatics.org/sms2/ident_sim.html)
679 (Stothard, 2000).
680
681 **Omics data integration into genome-scale models**
682 To investigate the impact of eATP on *E. coli* MG1655 metabolism in depth, a publicly
683 available genome-scale GEM called iML1515 (Monk *et al*, 2017) was utilised. Two
684 different growth media, M9 and LB, were separately considered, and the model was
685 adapted accordingly. We created a metabolic model for M9 using minimal growth
686 medium features/nutrition input values, which we referred to as M9GEM. For LB,
687 nutritional input values were assigned from a previous study (Marinos Kaleta &
688 Waschina, 2020), and the adapted model was called LBGEM. The REMI method
689 (Pandey Hadadi & Hatzimanikatis, 2019) was used to integrate genetic screen data
690 and metabolomics data into M9GEM and LBGEM, allowing for a better understanding
691 of the perturbation effect on metabolism while simultaneously integrating gene
692 expression and metabolomics data. REMI assumes that the reaction fluxes associated
693 with markedly regulated genes are deregulated, and it also integrates intracellular
694 metabolites by constraining reaction fluxes corresponding to differentially regulated
695 metabolites. The main goal of REMI is to ensure the consistency between gene
696 expression, metabolite concentrations, and reaction fluxes. To determine the specific
697 metabolic differences between two conditions (such as eATP and mock-treated
698 control), REMI creates a separate model for each condition and computes a maximum

consistency (MCS) score. This score reflects the number of genes/metabolites whose levels are consistent with fluxes, and the constraints can be incorporated into the model. To generate at least 20 alternative sets for the MCS from the given set of constraints, we employed mixed-integer linear programming (MILP). Due to the computational complexity of the optimization process, we selected 20 solutions for statistical analysis.

Differential reaction flux analysis

To quantify condition-specific changes in reaction fluxes, we obtained a score (R_i) for each reaction by utilizing the means and variances of flux distributions in eATP-treated and control conditions. To calculate scores for each reaction, we employed the REMI analysis approach (Pandey Hadadi & Hatzimanikatis, 2019), which involves considering alternative solutions of reaction fluxes for two conditions.

To identify markedly regulated reaction fluxes that were significantly altered, we utilized a cut-off of |Ri|>1. Additionally, we calculated *P* values using a nonparametric test, namely, the Wilcoxon signed rank test. We considered reactions with a *P* value <1e-3 to be significantly changed.

$$R_i = \frac{Mean_{eatp}(v_i) - Mean_{control}(v_i)}{\sqrt{Var_{eatp}(v_i) - Var_{control}(v_i)}}$$

Pathway and metabolic subsystem enrichment analysis

We conducted pathway enrichment analysis based on modulated genes and metabolites using KEGG pathways as the framework for analysis. To analyse metabolic subsystem enrichment based on metabolic reactions, we utilized GEM iML1515 (Monk *et al.*, 2017). To determine the significance of pathway or metabolic subsystems based on genes, metabolites, or reactions, we employed the hypergeometric probability density function (*P*), as defined by Equation (1):

$$P(\mathrm{k,N,K,n}) = \frac{\binom{K}{k}\binom{N-K}{n-k}}{\binom{N}{n}} \qquad (1)$$

where k and K represent the number of markedly regulated genes, metabolites, or reactions and the total number of genes/metabolites/reactions in a given pathway or metabolic subsystem, respectively. Variables n and N indicate the total number of markedly regulated genes, metabolites, or reactions in the given conditions and the total number of genes/metabolites/reactions in the organism and metabolic context, respectively.

To calculate the *p value* for each pathway or metabolic subsystem, we summed the probabilities for greater than or equal to the enriched number of markedly regulated genes, metabolites, or reactions (as shown in Equation 2):

$$pvalue = \sum_{k}^{K} P(x) \qquad (2)$$

Biomass building block analysis

Biomass building blocks (BBBs) are crucial components of genome-scale metabolic models that include amino acids, nucleotides, lipids, and other compounds required

for cellular growth and maintenance. We used flux balance analysis (FBA), a commonly used constraint-based method, to explore the dynamics of these building components under various environmental conditions. FBA allowed us to examine BBB fluxes in various media, including those subjected to eATP perturbations, providing vital insights into how an organism's metabolism adapts and responds to these changes.

Identification of metabolic subnetworks

To gain a more thorough understanding of the metabolic remodelling that results from exposure to eATP, we focused our efforts on identifying subnetworks containing both differentially regulated metabolites (DRMs) and differentially regulated reaction fluxes (DRFs). To accomplish this, we first removed co-factors from the network, as they can be involved in multiple metabolic reactions and can artificially inflate connectivity. This allowed us to better identify important metabolic subnetworks and reveal the true structure of the network. Additionally, we examined the first and second neighbour reactions of each DRM. First neighbour reactions are those that are directly involved with a metabolite's first neighbours, while second neighbour reactions involve the metabolite's second neighbours, which are not directly connected to the metabolite but are connected to its first neighbours. Finally, we analysed the most perturbed or deregulated reactions to identify the metabolic subnetworks where the most deregulation occurs in terms of both metabolites and reactions.

Statistical analysis

Except for the metabolomic analysis, which was performed using Metaboanalyst (5.0), all statistical analyses were performed in GraphPad Prism (version 9.0.2). The type of analysis and test of significance is mentioned in the respective figure legends. The default *P* value system of GraphPad Prism was used in all cases and is indicated in figure legends.

Source code availability

The script for metabolic modelling can be found at https://gitlab.com/obilab1/externalatpmets

Softwares used

The metabolomic analysis as performed with MetaboAnalyst 5.0 (Chong Wishart & Xia, 2019). For the visualisation of enrichment pathways and BBB analysis, Python (3.9) and R (4.2) were used. For modelling simulation, IBM CPLEX 12.9 MILP solver and MATLAB r2019a (The Mathworks, Natick, MA, USA) were used. The figures 4D and 5 were created with Illustrator.

Abbasian B, Shair A, O'Gorman DB, Pena-Diaz AM, Brennan L, Engelbrecht K, Koenig DW, Reid G, Burton JP (2019) Potential Role of Extracellular ATP Released by Bacteria in Bladder Infection and Contractility. *mSphere* 4: e00439-00419

Alvarez CL, Corradi G, Lauri N, Marginedas-Freixa I, Leal Denis MF, Enrique N, Mate SM, Milesi V, Ostuni MA, Herlax V, Schwarzbaum PJ (2017) Dynamic regulation of extracellular ATP in Escherichia coli. *The Biochemical journal* 474: 1395-1416

789 Arvidsson I, Tontanahal A, Johansson K, Kristoffersson AC, Kellnerová S, Berger M,
790 Dobrindt U, Karpman D (2022) Apyrase decreases phage induction and Shiga toxin
791 release from E. coli O157:H7 and has a protective effect during infection. *Gut Microbes*
792 14: 2122667
793 Atarashi K, Nishimura J, Shima T, Umesaki Y, Yamamoto M, Onoue M, Yagita H, Ishii
794 N, Evans R, Honda K, Takeda K (2008) ATP drives lamina propria T(H)17 cell
795 differentiation. *Nature* 455: 808-812
796 Baeza N, Mercade E (2021) Relationship Between Membrane Vesicles, Extracellular
797 ATP and Biofilm Formation in Antarctic Gram-Negative Bacteria. *Microb Ecol* 81: 645-
798 656
799 Berrier C, Coulombe A, Szabo I, Zoratti M, Ghazi A (1992) Gadolinium ion inhibits loss
800 of metabolites induced by osmotic shock and large stretch-activated channels in
801 bacteria. *European journal of biochemistry* 206: 559-565
802 Bours MJL, Swennen ELR, Di Virgilio F, Cronstein BN, Dagnelie PC (2006) Adenosine
803 5′-triphosphate and adenosine as endogenous signaling molecules in immunity and
804 inflammation. *Pharmacology & Therapeutics* 112: 358-404
805 Chang-Graham AL, Perry JL, Engevik MA, Engevik KA, Scribano FJ, Gebert JT,
806 Danhof HA, Nelson JC, Kellen JS, Strtak AC *et al* (2020) Rotavirus induces
807 intercellular calcium waves through ADP signaling. *Science* 370
808 Chen F, El-Naccache DW, Ponessa JJ, Lemenze A, Espinosa V, Wu W, Lothstein K,
809 Jin L, Antao O, Weinstein JS *et al* (2022) Helminth resistance is mediated by
810 differential activation of recruited monocyte-derived alveolar macrophages and
811 arginine depletion. *Cell Rep* 38: 110215
812 Chiaranunt P, Burrows K, Ngai L, Cao EY, Liang H, Tai SL, Streutker CJ, Girardin SE,
813 Mortha A (2022) NLRP1B and NLRP3 Control the Host Response following
814 Colonization with the Commensal Protist Tritrichomonas musculis. *Journal of*
815 *immunology (Baltimore, Md : 1950)* 208: 1782-1789
816 Chiaranunt P, Burrows K, Ngai L, Tai SL, Cao EY, Liang H, Hamidzada H, Wong A,
817 Gschwend J, Flüchter P *et al* (2023) Microbial energy metabolism fuels an intestinal
818 macrophage niche in solitary isolated lymphoid tissues through purinergic signaling.
819 *Sci Immunol* 8: eabq4573
820 Choi S, Choi E, Cho YJ, Nam D, Lee J, Lee EJ (2019) The Salmonella virulence
821 protein MgtC promotes phosphate uptake inside macrophages. *Nat Commun* 10: 3326
822 Chong J, Wishart DS, Xia J (2019) Using MetaboAnalyst 4.0 for Comprehensive and
823 Integrative Metabolomics Data Analysis. *Curr Protoc Bioinformatics* 68: e86
824 Covert MW, Palsson B (2002) Transcriptional regulation in constraints-based
825 metabolic models of Escherichia coli. *The Journal of biological chemistry* 277: 28058-
826 28064
827 Culp EJ, Goodman AL (2023) Cross-feeding in the gut microbiome: Ecology and
828 mechanisms. *Cell Host Microbe* 31: 485-499
829 Darfeuille-Michaud A, Neut C, Barnich N, Lederman E, Di Martino P, Desreumaux P,
830 Gambiez L, Joly B, Cortot A, Colombel JF (1998) Presence of adherent Escherichia
831 coli strains in ileal mucosa of patients with Crohn's disease. *Gastroenterology* 115:
832 1405-1413
833 Datsenko KA, Wanner BL (2000) One-step inactivation of chromosomal genes in
834 Escherichia coli K-12 using PCR products. *Proc Natl Acad Sci USA* 97
835 Deiwick J, Nikolaus T, Erdogan S, Hensel M (1999) Environmental regulation of
836 Salmonella pathogenicity island 2 gene expression. *Mol Microbiol* 31: 1759-1773

Di Virgilio F, Pinton P, Falzoni S (2016) Assessing Extracellular ATP as Danger Signal In Vivo: The pmeLuc System. *Methods in molecular biology (Clifton, NJ)* 1417: 115-129

Ding Q, Quah SY, Tan KS (2016) Secreted adenosine triphosphate from Aggregatibacter actinomycetemcomitans triggers chemokine response. *Mol oral Microbiol* 31: 423-434

Ding Q, Tan KS (2016) The Danger Signal Extracellular ATP Is an Inducer of Fusobacterium nucleatum Biofilm Dispersal. *Front Cell Infect Microbiol* 6: 155

Ellermeier CD, Ellermeier JR, Slauch JM (2005) HilD, HilC and RtsA constitute a feed forward loop that controls expression of the SPI1 type three secretion system regulator hilA in Salmonella enterica serovar Typhimurium. *Mol Microbiol* 57: 691-705

Gerlach RG, Hölzer SU, Jäckel D, Hensel M (2007) Rapid Engineering of Bacterial Reporter Gene Fusions by Using Red Recombination. *Appl Environ Microbiol* 73: 4234-4242

Gerosa L, Sauer U (2011) Regulation and control of metabolic fluxes in microbes. *Curr Opin Biotechnol* 22: 566-575

Gianchandani EP, Joyce AR, Palsson B, Papin JA (2009) Functional states of the genome-scale Escherichia coli transcriptional regulatory system. *PLoS computational biology* 5: e1000403

Hironaka I, Iwase T, Sugimoto S, Okuda K, Tajima A, Yanaga K, Mizunoe Y (2013) Glucose triggers ATP secretion from bacteria in a growth-phase-dependent manner. *Appl Environ Microbiol* 79: 2328-2335

Huang da W, Sherman BT, Lempicki RA (2009) Systematic and integrative analysis of large gene lists using DAVID bioinformatics resources. *Nature protocols* 4: 44-57

Idzko M, Ferrari D, Eltzschig HK (2014) Nucleotide signalling during inflammation. *Nature* 509: 310-317

Idzko M, Hammad H, van Nimwegen M, Kool M, Willart MA, Muskens F, Hoogsteden HC, Luttmann W, Ferrari D, Di Virgilio F *et al* (2007) Extracellular ATP triggers and maintains asthmatic airway inflammation by activating dendritic cells. *Nat Med* 13: 913-919

Ihssen J, Jovanovic N, Sirec T, Spitz U (2021) Real-time monitoring of extracellular ATP in bacterial cultures using thermostable luciferase. *PLOS ONE* 16: e0244200

Ivanova EP, Alexeeva YV, Pham DK, Wright JP, Nicolau DV (2006) ATP level variations in heterotrophic bacteria during attachment on hydrophilic and hydrophobic surfaces. *International microbiology : the official journal of the Spanish Society for Microbiology* 9: 37-46

Iwase T, Shinji H, Tajima A, Sato F, Tamura T, Iwamoto T, Yoneda M, Mizunoe Y (2010) Isolation and identification of ATP-secreting bacteria from mice and humans. *J Clin Microbiol* 48: 1949-1951

Krautkramer KA, Fan J, Bäckhed F (2021) Gut microbial metabolites as multi-kingdom intermediates. *Nat Rev Microbiol* 19: 77-94

Kurashima Y, Amiya T, Nochi T, Fujisawa K, Haraguchi T, Iba H, Tsutsui H, Sato S, Nakajima S, Iijima H *et al* (2012) Extracellular ATP mediates mast cell-dependent intestinal inflammation through P2X7 purinoceptors. *Nat Commun* 3: 1034

Kusu T, Kayama H, Kinoshita M, Jeon SG, Ueda Y, Goto Y, Okumura R, Saiga H, Kurakawa T, Ikeda K *et al* (2013) Ecto-nucleoside triphosphate diphosphohydrolase 7 controls Th17 cell responses through regulation of luminal ATP in the small intestine. *Journal of immunology (Baltimore, Md : 1950)* 190: 774-783

Letunic I, Bork P (2021) Interactive Tree Of Life (iTOL) v5: an online tool for phylogenetic tree display and annotation. *Nucleic Acids Res* 49: W293-w296

887 Li M, Chen Y, Wu S, Tang Y, Deng Y, Yuan J, Dong J, Li H, Tang L (2016) TmcN is
888 involved in ATP regulation of tautomycetin biosynthesis in Streptomyces
889 griseochromogenes. *Biochem Biophys Res Commun* 478: 221-226
890 Li M, Kim TJ, Kwon HJ, Suh JW (2008) Effects of extracellular ATP on the physiology
891 of Streptomyces coelicolor A3(2). *FEMS Microbiol Lett* 286: 24-31
892 Li M, Lee SK, Yang SH, Ko JH, Han JS, Kim TJ, Suh JW (2011) ATP modulates the
893 growth of specific microbial strains. *Curr Microbiol* 62: 84-89
894 Li XP, Zhou LL, Guo YH, Wang JW (2021) The signaling role of extracellular ATP in
895 co-culture of Shiraia sp. S9 and Pseudomonas fulva SB1 for enhancing hypocrellin A
896 production. *Microbial cell factories* 20: 144
897 Lou L, Zhang P, Piao R, Wang Y (2019) Salmonella Pathogenicity Island 1 (SPI-1)
898 and Its Complex Regulatory Network. *Front Cell Infect Microbiol* 9: 270
899 Malik-Kale P, Winfree S, Steele-Mortimer O (2012) The bimodal lifestyle of intracellular
900 Salmonella in epithelial cells: replication in the cytosol obscures defects in vacuolar
901 replication. *PLOS ONE* 7: e38732
902 Malo MS, Moaven O, Muhammad N, Biswas B, Alam SN, Economopoulos KP, Gul
903 SS, Hamarneh SR, Malo NS, Teshager A *et al* (2014) Intestinal alkaline phosphatase
904 promotes gut bacterial growth by reducing the concentration of luminal nucleotide
905 triphosphates. *Am J Physiol Gastrointest Liver Physiol* 306: G826-838
906 Marinos G, Kaleta C, Waschina S (2020) Defining the nutritional input for genome-
907 scale metabolic models: A roadmap. *PLOS ONE* 15: e0236890
908 Marteyn B, West NP, Browning DF, Cole JA, Shaw JG, Palm F, Mounier J, Prévost
909 MC, Sansonetti P, Tang CM (2010) Modulation of Shigella virulence in response to
910 available oxygen in vivo. *Nature* 465: 355-358
911 McDonough KA, Rodriguez A (2011) The myriad roles of cyclic AMP in microbial
912 pathogens: from signal to sword. *Nat Rev Microbiol* 10: 27-38
913 Medina-Castellanos E, Esquivel-Naranjo EU, Heil M, Herrera-Estrella A (2014)
914 Extracellular ATP activates MAPK and ROS signaling during injury response in the
915 fungus Trichoderma atroviride. *Frontiers in plant science* 5: 659
916 Medina-Castellanos E, Villalobos-Escobedo JM, Riquelme M, Read ND, Abreu-
917 Goodger C, Herrera-Estrella A (2018) Danger signals activate a putative innate
918 immune system during regeneration in a filamentous fungus. *PLOS Genet* 14:
919 e1007390
920 Mempin R, Tran H, Chen C, Gong H, Kim Ho K, Lu S (2013) Release of extracellular
921 ATP by bacteria during growth. *BMC Microbiol* 13: 301
922 Meng L, Li M, Yang SH, Kim TJ, Suh JW (2011) Intracellular ATP levels affect
923 secondary metabolite production in Streptomyces spp. *Bioscience, biotechnology, and*
924 *biochemistry* 75: 1576-1581
925 Mi H, Muruganujan A, Casagrande JT, Thomas PD (2013) Large-scale gene function
926 analysis with the PANTHER classification system. *Nature protocols* 8: 1551-1566
927 Mitosch K, Beyß M, Phapale P, Drotleff B, Nöh K, Alexandrov T, Patil KR, Typas A
928 (2023) A pathogen-specific isotope tracing approach reveals metabolic activities and
929 fluxes of intracellular Salmonella. *PLOS Biol* 21: e3002198
930 Monk JM, Lloyd CJ, Brunk E, Mih N, Sastry A, King Z, Takeuchi R, Nomura W, Zhang
931 Z, Mori H *et al* (2017) iML1515, a knowledgebase that computes Escherichia coli traits.
932 *Nat Biotechnol* 35: 904-908
933 Nilsson L (1978) New rapid bioassay of gentamicin based on luciferase assay of
934 extracellular ATP in bacterial cultures. *Antimicrob Agents Chemother* 14: 812-816

935 Nolan LM, Cavaliere R, Turnbull L, Whitchurch CB (2015) Extracellular ATP inhibits
936 twitching motility-mediated biofilm expansion by Pseudomonas aeruginosa. *BMC*
937 *Microbiol* 15: 55
938 Nougayrède J-P, Homburg S, Taieb F, Boury M, Brzuszkiewicz E, Gottschalk G,
939 Buchrieser C, Hacker J, Dobrindt U, Oswald E (2006) Escherichia coli Induces DNA
940 Double-Strand Breaks in Eukaryotic Cells. *Science* 313: 848-851
941 Pandey V, Hadadi N, Hatzimanikatis V (2019) Enhanced flux prediction by integrating
942 relative expression and relative metabolite abundance into thermodynamically
943 consistent metabolic models. *PLoS computational biology* 15: e1007036
944 Patel BA (2014) Mucosal adenosine triphosphate mediates serotonin release from
945 ileal but not colonic guinea pig enterochromaffin cells. *Neurogastroenterology and*
946 *motility : the official journal of the European Gastrointestinal Motility Society* 26: 237-
947 246
948 Perruzza L, Gargari G, Proietti M, Fosso B, D'Erchia AM, Faliti CE, Rezzonico-Jost T,
949 Scribano D, Mauri L, Colombo D *et al* (2017) T Follicular Helper Cells Promote a
950 Beneficial Gut Ecosystem for Host Metabolic Homeostasis by Sensing Microbiota-
951 Derived Extracellular ATP. *Cell Rep* 18: 2566-2575
952 Pham AQ, Cho SH, Nguyen CT, Stacey G (2020) Arabidopsis Lectin Receptor Kinase
953 P2K2 Is a Second Plant Receptor for Extracellular ATP and Contributes to Innate
954 Immunity. *Plant Physiol* 183: 1364-1375
955 Platenkamp A, Mellies JL (2018) Environment Controls LEE Regulation in
956 Enteropathogenic Escherichia coli. *Front Microbiol* 9: 1694
957 Proietti M, Perruzza L, Scribano D, Pellegrini G, D'Antuono R, Strati F, Raffaelli M,
958 Gonzalez SF, Thelen M, Hardt WD *et al* (2019) ATP released by intestinal bacteria
959 limits the generation of protective IgA against enteropathogens. *Nat Commun* 10: 250
960 Puhar A, Tronchère H, Payrastre B, Tran Van Nhieu G, Sansonetti Philippe J (2013)
961 A Shigella Effector Dampens Inflammation by Regulating Epithelial Release of Danger
962 Signal ATP through Production of the Lipid Mediator PtdIns5P. *Immunity* 39: 1121-
963 1131
964 Qiu H, Pu F, Liu Z, Deng Q, Sun P, Ren J, Qu X (2019) Depriving Bacterial Adhesion-
965 Related Molecule to Inhibit Biofilm Formation Using CeO2 -Decorated Metal-Organic
966 Frameworks. *Small (Weinheim an der Bergstrasse, Germany)*: e1902522
967 Raffelsberger N, Hetland MAK, Svendsen K, Småbrekke L, Löhr IH, Andreassen LLE,
968 Brisse S, Holt KE, Sundsfjord A, Samuelsen Ø, Gravningen K (2021) Gastrointestinal
969 carriage of Klebsiella pneumoniae in a general adult population: a cross-sectional
970 study of risk factors and bacterial genomic diversity. *Gut Microbes* 13: 1939599
971 Rooks MG, Veiga P, Reeves AZ, Lavoie S, Yasuda K, Asano Y, Yoshihara K, Michaud
972 M, Wardwell-Scott L, Gallini CA *et al* (2017) QseC inhibition as an antivirulence
973 approach for colitis-associated bacteria. *Proc Natl Acad Sci U S A* 114: 142-147
974 Scott BM, Gutiérrez-Vázquez C, Sanmarco LM, da Silva Pereira JA, Li Z, Plasencia
975 A, Hewson P, Cox LM, O'Brien M, Chen SK *et al* (2021) Self-tunable engineered yeast
976 probiotics for the treatment of inflammatory bowel disease. *Nat Med* 27: 1212-1222
977 Stothard P (2000) The sequence manipulation suite: JavaScript programs for
978 analyzing and formatting protein and DNA sequences. *BioTechniques* 28: 1102, 1104
979 Tadala L, Langenbach D, Dannborg M, Cervantes-Rivera R, Sharma A, Vieth K,
980 Rieckmann LM, Wanders A, Cisneros DA, Puhar A (2022) Infection-induced
981 membrane ruffling initiates danger and immune signaling via the mechanosensor
982 PIEZO1. *Cell Rep* 40: 111173

983 Takemura N, Kurashima Y, Mori Y, Okada K, Ogino T, Osawa H, Matsuno H, Aayam
984 L, Kaneto S, Park EJ *et al* (2018) Eosinophil depletion suppresses radiation-induced
985 small intestinal fibrosis. *Sci Transl Med* 10
986 Tanaka K, Choi J, Cao Y, Stacey G (2014) Extracellular ATP acts as a damage-
987 associated molecular pattern (DAMP) signal in plants. *Frontiers in plant science* 5: 446
988 Tani H, Li B, Kusu T, Okumura R, Nishimura J, Okuzaki D, Motooka D, Arakawa S,
989 Mori A, Yoshihara T *et al* (2021) The ATP-hydrolyzing ectoenzyme E-NTPD8
990 attenuates colitis through modulation of P2X4 receptor-dependent metabolism in
991 myeloid cells. *Proc Natl Acad Sci U S A* 118
992 Tatano Y, Kanehiro Y, Sano C, Shimizu T, Tomioka H (2015) ATP exhibits
993 antimicrobial action by inhibiting bacterial utilization of ferric ions. *Sci Rep* 5: 8610
994 Thomas PD, Campbell MJ, Kejariwal A, Mi H, Karlak B, Daverman R, Diemer K,
995 Muruganujan A, Narechania A (2003) PANTHER: a library of protein families and
996 subfamilies indexed by function. *Genome Res* 13: 2129-2141
997 Tjaden J, Schwöppe C, Möhlmann T, Quick PW, Neuhaus HE (1998) Expression of a
998 plastidic ATP/ADP transporter gene in Escherichia coli leads to a functional adenine
999 nucleotide transport system in the bacterial cytoplasmic membrane. *The Journal of*
1000 *biological chemistry* 273: 9630-9636
1001 Valat C, Champiat D, N'Guyen TT, Loiseau G, Raimbault M, Montet D (2003) Use of
1002 ATP bioluminescence to determine the bacterial sensitivity threshold to a bacteriocin.
1003 *Luminescence* 18: 254-258
1004 Verkhratsky A, Burnstock G (2014) Biology of purinergic signalling: its ancient
1005 evolutionary roots, its omnipresence and its multiple functional significance.
1006 *BioEssays : news and reviews in molecular, cellular and developmental biology* 36:
1007 697-705
1008 Wallenstein A, Rehm N, Brinkmann M, Selle M, Bossuet-Greif N, Sauer D, Bunk B,
1009 Spröer C, Wami HT, Homburg S *et al* (2020) ClbR Is the Key Transcriptional Activator
1010 of Colibactin Gene Expression in Escherichia coli. *mSphere* 5: e00591-00520
1011 Wan P, Liu X, Xiong Y, Ren Y, Chen J, Lu N, Guo Y, Bai A (2016) Extracellular ATP
1012 mediates inflammatory responses in colitis via P2 x 7 receptor signaling. *Sci Rep* 6:
1013 19108
1014 Wilhelm K, Ganesan J, Müller T, Dürr C, Grimm M, Beilhack A, Krempl CD, Sorichter
1015 S, Gerlach UV, Jüttner E *et al* (2010) Graft-versus-host disease is enhanced by
1016 extracellular ATP activating P2X7R. *Nat Med* 16: 1434-1438
1017 Xi C, Wu J (2010) dATP/ATP, a multifunctional nucleotide, stimulates bacterial cell
1018 lysis, extracellular DNA release and biofilm development. *PLOS ONE* 5: e13355
1019 Yu Lomakina G, Ugarova NN (2022) Application of Bioluminescent Methods to Study
1020 the Effect of the Membrane-active Antibiotic Colistin on Bacterial Cells. *Photochem*
1021 *Photobiol* 98: 1077-1083
1022 Zaslaver A, Bren A, Ronen M, Itzkovitz S, Kikoin I, Shavit S, Liebermeister W, Surette
1023 MG, Alon U (2006) A comprehensive library of fluorescent transcriptional reporters for
1024 Escherichia coli. *Nature methods* 3: 623-628
1025
1026 Figure Legends
1027
1028 **Figure 1. eATP triggers a strong dose-, medium- and time- dependent**
1029 **transcriptional response in non-pathogenic *E. coli*.**
1030 **A** and **C**, Number of eATP-regulated promoters in percentage with respect to
1031 unstimulated controls from fluorescence reporter screens (n=2) performed in LB or
1032 minimal medium M9 in *E. coli* MG1655, 180 min after addition of 1 mM ATP.

1033 **B** and **D**, Log fold change of promoter activity upon exposure to 1 mM eATP 180 min
1034 after ATP addition in LB or M9 in *E. coli* MG1655, shown as mean of independent
1035 experiments (n≥2).
1036 **E**-**G**, Comparison of the number of (**E**) all differentially expressed promoters in *E. coli*
1037 MG1655, (**F**) all up-regulated promoters, and (**G**) all down-regulated promoters 180
1038 min after addition of 1 mM ATP in LB or M9.
1039 **H**-**M**, Promoter activity of selected up-regulated promoters P*ybjX*, P*gadW* and P*rstA*
1040 controlling the expression of the reporter GFP in the presence of increasing
1041 concentrations of added ATP in *E. coli* MG1655. Strains were grown in LB (upper
1042 panels) or M9 (lower panels). Shown is the ratio of GFP fluorescence to the number
1043 of bacteria determined by absorbance at 600 nm over time (columns representing the
1044 mean with s.e.m, left Y axes), as well as the bacterial growth (continuous lines
1045 representing means with s.e.m, right Y axes). Statistical analysis: two-way ANOVA
1046 with Dunnett's multiple comparison test; *P < 0.05, **P < 0.01, ***P < 0.001 and ****P
1047 < 0.0001; ns, not significant.
1048
1049 **Figure 2. Pathway analysis of the eATP-triggered transcriptional response in**
1050 **non-pathogenic *E. coli*.**
1051 **A**-**B**, KEGG pathway enrichment analysis on the up- and down-regulated genes in LB
1052 or M9 180 min after 1 mM ATP addition in comparison to unstimulated bacteria.
1053 **C**, Gene ontology analysis using the PANTHER classification system of up- or down-
1054 regulated genes in LB and M9. Processes with a P value < $1x10^{-3}$ are shown.
1055
1056 **Figure 3. eATP triggers a strong metabolic response in non-pathogenic *E. coli*.**
1057 **A**, Comparison of the total number of common or unique detected metabolites from *E.*
1058 *coli* MG1655 grown in LB or M9 after 180 min in the presence of 1 mM added ATP.
1059 LB pellet: n=3 and 57 metabolites, M9 pellet: n=4 and 53 metabolites, M9 supernatant:
1060 n=3 and 89 metabolites.
1061 **B**-**D**, Partial Least Squares discriminant analysis (PLS-DA) scores plots of
1062 components one and two, comparing metabolomic samples from *E. coli* MG1655
1063 treated with 1 mM ATP for 180 min versus the unstimulated control in (**B**) the pellet in
1064 LB (n=3), (**C**) the pellet in M9 (n=4), and (**D**) the supernatant in M9 (n=3).
1065 **E**, Comparison of fold changes in abundance of top 25 metabolites based on PLS-DA
1066 analysis from samples in (**B**).
1067 **F**, Comparison of changes in abundance of top 25 metabolites based on PLS-DA
1068 analysis from samples in (**C**).
1069 **G**, Comparison of fold changes in abundance of top 25 metabolites based on PLS-DA
1070 analysis from samples in (**D**).
1071 **H**-**J**, Changes of relative concentrations of selected modulated intracellular
1072 metabolites from samples in (**B** and **D**) and extracellular metabolites from samples in
1073 (**D**). The boxplots show the normalised values (mean and s.d.). The Y-axis represents
1074 the normalised peak area of metabolites. Black dots represent the normalised
1075 concentrations of all samples of each metabolite. The notch indicates the 95%
1076 confidence interval around the median. The mean concentration of each group is
1077 shown by a yellow diamond. Statistical analysis: two-sided Welch's t test; raw P-values
1078 are indicated in each panel.
1079
1080 **Figure 4. Model-based enrichment analysis of predicted reaction fluxes and**
1081 **analysis of biomass building blocks triggered by eATP in non-pathogenic *E.***
1082 ***coli*.**

A, Metabolic subsystems enrichment analysis for *E. coli* MG1655 stimulated with 1 mM eATP for 180 min in rich (LB) medium using differentially regulated reactions (DERs).
B, Metabolic subsystems enrichment analysis for *E. coli* MG1655 stimulated with 1 mM eATP for 180 min in minimal (M9) medium using differentially regulated reactions (DERs).
C, Differential fold changes of *in silico* production for eight biomass building block groups between *E. coli* MG1655 grown in rich (LB) and minimal (M9) medium in presence of 1 mM eATP for 180 min *versus* the unstimulated control. Each dot is an alternative solution predicted by the genome-scale metabolic model. A cut-off P-value <0,05 was used.
D, Identification of metabolic subnetworks based on differentially regulated reactions and differentially regulated intracellular metabolites triggered in *E. coli* MG1655 by addition of 1 mM ATP for 180 min in LB (n=3). Shown are the differentially regulated intracellular metabolites (labelled in red, fold change >1,5, see also Fig **3H**), modulated genes (labelled in orange, fold change >1,5, Table EV1) and differentially regulated reactions (labelled in capital purple and black circles, P-value < 1e-3). Other compounds are labelled in orange circles and written in black. Non-modulated reactions are labelled in capital grey and black circles. TRPtipp, L-tryptophan transport out (periplasm); INSH, Inosine hydrolase; UMPK, UMP kinase; GALUi, UTP-glucose-1-phosphate uridylyltransferase (irreversible).

Figure 5. Metabolic subnetwork analysis integrating transcriptional and metabolic changes triggered by eATP in non-pathogenic *E. coli* in M9.
Identification of metabolic subnetworks based on differentially regulated reactions and differentially regulated intracellular metabolites triggered in *E. coli* MG1655 by addition of 1 mM ATP for 180 min M9 (n=4). Shown are the differentially regulated intracellular metabolites (labelled in red, fold change >1,5, see also Fig **3I**), modulated genes (labelled in orange, fold change >1,5, Table EV1) and differentially regulated reactions (labelled in capital purple and black circles, P-value < 1e-3). Other compounds are labelled in orange circles and written in black. Non-modulated reactions are labelled in capital grey and black circles. DADA, Deoxyadenosine deaminase; PUNP6, Purine-nucleoside phosphorylase (Deoxyinosine); GLUPRT, Glutamine phosphoribosyldiphosphate amidotransferase; ACGS, N-acetylglutamate synthase; GTHS, Glutathione synthetase; NNAM, Nicotinamidase; CYTDK2, Cytidine kinase (GTP); TKT1, Transketolase; AMPN, AMP nucleosidase; PUNP2, Purine-nucleoside phosphorylase (Deoxyadenosine).

Figure 6. eATP alters antibiotics and antimicrobial peptides susceptibility, triggers a transcriptional response in several Enterobacteriacae and regulates the expression of virulence factors.
A, Relative antibiotic sensitivity of *E. coli* MG1655 grown on LB compared to LB + 1mM ATP plates in the presence of ampicillin (AMP), fosfomycin (FOS), aztreonam (ATM), ceftazidime (CAZ), imipenem (IMI), cefazolin (KZ), mecillinam (MEC), gentamicin (CN), plazomicin (PLZ), or ciprofloxacin (CIP). Shown is the mean with s.d. of 3 independent experiments. Statistical analysis: multiple t-test; *P < 0.05; ns, not significant.
B-H, Growth of *E. coli* MG1655 in LB upon treatment at time 0 with antimicrobial peptides or vehicle in the presence or absence of 1 mM ATP. Shown is the mean with s.d. of 3 independent experiments performed in duplicates or triplicates. Statistical

analysis: two-way ANOVA with Dunnett's multiple comparison test; *P < 0.05, **P < 0.01, ***P < 0.001 and ****P < 0.0001; ns, not significant.

I, Response ratio to eATP in percentage in selected bacteria transformed with reporter plasmids encoding promoters that upregulate the expression of GFP in eATP-treated commensal *E. coli* MG1655, which was used as reference (100%). Bacteria were stimulated with 1 mM ATP for 180 min in LB or M9. Shown is the average ratio calculated from at least 3 independent experiments performed in triplicates.

J-M, Promoter activity of selected virulence or fitness factors seen as GFP expression normalised to number of bacteria upon addition of increasing concentrations of ATP for 180 min in LB. Indicated promoter regions were cloned into GFP reporter plasmids and transformed into indicated corresponding strains. Increasing concentrations of eATP were added and the expression ratio was calculated comparing the fluorescence/OD_{600nm} in LB without ATP with fluorescence/OD_{600nm} in LB + ATP. Shown is the mean with s.e.m. of ≥ 3 independent experiments performed in duplicates or triplicates. Statistical analysis: two-way ANOVA with Dunnett's multiple comparison test; *P < 0.05, **P < 0.01, ***P < 0.001 and ****P < 0.0001; ns, not significant.

Expanded View Figure Legends

Expanded view Fig 1. eATP triggers a strong transcriptional response in non-pathogenic *E. coli*, related to Fig 1.

A, Overview of the protocol for the promoter library screening for a transcriptional response to eATP. Created using BioRender.com.

B-G, Activity of indicated promoters controlling the expression of the reporter GFP (plasmid construct) in the presence or absence of 1 mM ATP obtained in LB (upper panels) or M9 (lower panels). Shown is the ratio of GFP fluorescence to number of bacteria determined by absorbance at 600 nm over time (columns representing the mean with s.e.m, left Y axes), as well as the bacterial growth (continuous lines representing means with s.e.m, right Y axes).

H, Day-to-day reproducibility for a set of 96 random samples. Shown is the GFP fluorescence divided by the number of bacteria determined by absorbance at 600 nm in LB measured on day 1 and day 2.

I, Growth curves of *E. coli* MG1655 over 240 min with (blue line) or without (orange line) 1mM ATP addition in LB obtained for a set of 2 random plates from the library. The continuous lines represent the mean absorbance and the colour-matched shaded areas the s.e.m.

J, Bacterial counts determined by plating before and 180 min after 1 mM ATP addition in LB.

K, Same as in (**I**) but in M9.

L, Same as in (**J**) but in M9.

M, Promoter activity of MG1655 carrying the P*gadW*-mEGFP chromosomal fusion in the presence and absence of 1 mM ATP obtained as in **B-G**. The mean fluorescence value of the unstimulated control at 0 min was set to 1 to calculate relative changes of the fluorescence. The activity of the *gadW* promoter obtained using the reporter plasmid is shown in Fig **1I** for comparison.

N, Promoter activity (GFP/OD_{600nm}) of the reporter plasmid encoding P*cbpA-gfp* in the presence of 1mM ATP in *E. coli* MG1655.

O, Promoter activity of *E. coli* MG1655 carrying the P*cbpA*-mEGFP chromosomal fusion in the presence and absence of 1 mM ATP obtained as in **B-G**. The mean fluorescence value of the unstimulated control at 0 min was set to 1 to calculate relative changes of the fluorescence. The activity of the *cbpA* promoter obtained using the reporter plasmid is shown in Fig **1I** for comparison.
Statistical analysis: two-way ANOVA with Dunnett's multiple comparison test; *P < 0.05, **P < 0.01, ***P < 0.001 and ****P < 0.0001; ns, not significant.

Expanded view Fig 2. eATP triggers a strong metabolic response in non-pathogenic *E. coli* related to Fig 3.
A, Volcano plot analysis of intracellular metabolites changes after addition of 1 mM ATP in LB. Fold change (FC) ≥ 1.5 or ≤0.5 ($p \leq 0.05$) is considered significant.
B, VIP (Variable Importance in Projection) score of PLS-DA analysis from samples in (**A**).
C, Volcano plot analysis of intracellular metabolites changes after addition of 1 mM ATP in M9. Fold change (FC) ≥ 1.5 or ≤0.5 ($p \leq 0.05$) is considered significant.
D, VIP score of PLS-DA analysis from samples in (**C**).
E, Volcano plot analysis of extracellular metabolites changes after addition of 1 mM ATP in M9. Fold change (FC) ≥ 1.5 or ≤0.5 ($p \leq 0.05$) is considered significant.
F, VIP score of PLS-DA analysis from samples in (**E**).

Expanded view Fig 3. Modulated intracellular metabolites upon exposure to 100 μM ATP in M9 in non-pathogenic *E. coli*, related to Fig 3.
A, PLS-DA scores plots of components one and two, comparing metabolomic samples (pellet) from treatment with 100 μM ATP for 180 min versus the unstimulated controls (n=3).
B, Comparison of fold changes in abundance of top 25 metabolites based on PLS-DA analysis from samples in (**A**).
C, Volcano plot analysis of intracellular metabolites changes from samples in (**A**). Fold change (FC) ≥ 1.5 or ≤0.5 ($p \leq 0.05$) is considered significant.
D, VIP (Variable Importance in Projection) score of PLS-DA analysis from samples in (**A**).
E, Boxplots of relative concentrations of selected modulated intracellular metabolites from samples in (**A**). The bar plots show the normalised values (mean with s.d.). The Y-axis represents normalised peak area of metabolites. Black dots represent the normalised concentrations of all samples of each metabolite. The notch indicates the 95% confidence interval around the median. The mean concentration of each group is shown by a yellow diamond. Statistical analysis: two-sided Welch's t test; raw P-values are indicated in each panel.
F, KEGG pathway enrichment analysis of the up- and down-regulated intracellular metabolites in M9 180 min after 100 μM ATP addition in comparison to unstimulated bacteria.
G, Comparison of the number of all measured intracellular metabolites in *E. coli* MG1655 180 min after addition of 1 mM or 100 μM ATP M9 medium.
H, Comparison of the number of all modulated intracellular metabolites in *E. coli* MG1655 180 min after addition of 1 mM or 100 μM ATP M9 medium.

Expanded view Fig 4. eATP enhances antimicrobial peptide susceptibility, related to Fig 6.

1231 **A-G**, Growth of *E. coli* MG1655 in LB upon treatment at time 0 with antimicrobial
1232 peptides or vehicle in the presence or absence of 1 mM ATP. Shown is the mean with
1233 s.d. of 3 independent experiments performed in duplicates or triplicates. Statistical
1234 analysis: two-way ANOVA with Dunnett's multiple comparison test; *P < 0.05; **P <
1235 0.01, ***P < 0.001 and ****P < 0.0001; ns, not significant.
1236
1237 **Expanded view Fig 5. eATP triggers a transcriptional response in non-**
1238 **pathogenic, pathobiontic or pathogenic bacteria and regulates the expression**
1239 **of virulence factors, related to Fig 6.**
1240 **A**, Sequence similarity in percentage of promoters P*gadW*, P*ybjX*, P*rstA* and P*slyB*
1241 promoters in the indicated bacteria compared to *E. coli* MG1655.
1242 **B**, Promoter activity of the promoter P*rstA* controlling the expression of the reporter
1243 GFP in the presence and absence of 1 mM ATP in indicated strains grown in LB, as
1244 in Fig **6A**. Shown is the ratio of GFP fluorescence to number of bacteria determined
1245 by the absorbance at 600 nm over time (columns representing the mean with s.e.m of
1246 3 independent experiments performed in triplicates, left Y axes), as well as the
1247 bacterial growth (continuous lines representing means with s.e.m, right Y axes).
1248 Statistical analysis: two-way ANOVA with Dunnett's multiple comparison test; *P <
1249 0.05, **P < 0.01, ***P < 0.001 and ****P < 0.0001; ns, not significant.
1250 **C-D**, Promoter activity of selected virulence or fitness factors seen as GFP expression
1251 normalised to number of bacteria upon addition of increasing concentrations of ATP
1252 for 180 min in LB. The expression ratio was calculated comparing the
1253 fluorescence/OD_{600nm} in LB without ATP with fluorescence/OD_{600nm} in LB + ATP.
1254 Shown is the mean with s.e.m. of ≥ 3 independent experiments performed in
1255 duplicates or triplicates. Statistical analysis: two-way ANOVA with Dunnett's multiple
1256 comparison test; ns, not significant.
1257
1258 Expanded view Tables legend
1259
1260 **Expanded view Table 1: Transcriptional reporter library screening**
1261 Screening_LB: Summary of the data from the transcriptional library screening in LB.
1262 Shown is the average GFP fluorescence divided by OD_{600nm} of at least 2 biological
1263 replicates for each time point (0, 5, 30, 60, 120 and 180 min after ATP addition), the
1264 fluorescence ratio between the eATP-treated and the mock-treated samples and the
1265 log_2 of this ratio.
1266 Screening_M9: Same as aforementioned but in M9.
1267 Panther analysis: Results from the Panther analysis in LB and M9 of differentially
1268 expressed genes (DEGs, FC>1,5) upon exposure to 1 mM ATP for 180 min.
1269 LB_genes_KEGG: Pathway enrichment analysis based on differentially expressed
1270 genes upon exposure to 1 mM ATP in LB for 180 min.
1271 M9_genes_KEGG: Pathway enrichment analysis based on differentially expressed
1272 genes upon exposure to 1 mM ATP in M9 for 180 min.
1273
1274 **Expanded view Table 2: Metabolomic data**
1275 Metabolites_LC_MS: Summary of all metabolites identified in *E. coli* MG1655 upon
1276 exposure to 100 µM or 1 mM ATP for 180 min and their associated FC and P-value
1277 compared to mock-treated bacteria.
1278 Metabolites_role: Summary of modulated bioactive metabolites and their roles.
1279
1280 **Expanded view Table 3: Metabolic and flux modelling**

M9_diff_flux: List of reaction fluxes identified in *E. coli* MG1655 upon addition of 1 mM ATP for 180 min in M9.
M9_flux_enrichment: Metabolic subsystems enrichment analysis for *E. coli* MG1655 stimulated with 1 mM ATP for 180 min in M9 using differentially regulated reactions (DERs).
M9_BBB: List of the tested biomass building blocks (BBBs) and their associated production rate ratio in eATP-treated compared to mock-treated bacteria in M9 upon exposure to eATP for 180min.
LB_diff_flux List of reaction fluxes identified in *E. coli* MG1655 upon addition of 1 mM ATP for 180 min in M9.
LB_flux_enrichment: Metabolic subsystems enrichment analysis for *E. coli* MG1655 stimulated with 1 mM ATP for 180 min in LB using differentially regulated reactions (DERs).
LB_BBB: List of the tested biomass building blocks and their associated production rate ratio between the eATP treated bacteria and the mock in LB upon exposure to eATP for 180min.

Expanded view Table: Strains, plasmids, and primers
Strains: List of bacterial strains used in the study.
Plasmids: List of plasmids used in the study.
Primers: List of the primers used in the study.

Expanded view Table: List of antibiotics and antimicrobial peptides used in the study
Antibiotics: List of antibiotics used in the study and the MIC obtained on LB agar and LB agar supplemented with 1mM ATP.
AMPs: List of antimicrobial peptides used in the study.

References Expanded view Figures and Tables.

Allaoui, A., J. Mounier, M. C. Prévost, P. J. Sansonetti, and C. Parsot. 1992. 'icsB: a Shigella flexneri virulence gene necessary for the lysis of protrusions during intercellular spread', *Mol Microbiol*, 6: 1605-16.
Baba, T., T. Ara, M. Hasegawa, Y. Takai, Y. Okumura, M. Baba, K. A. Datsenko, M. Tomita, B. L. Wanner, and H. Mori. 2006. 'Construction of Escherichia coli K-12 in-frame, single-gene knockout mutants: the Keio collection', *Mol Syst Biol*, 2.
Bassil, A. K., S. Bourdu, K. A. Townson, A. Wheeldon, E. M. Jarvie, N. Zebda, A. Abuin, E. Grau, G. P. Livi, L. Punter, J. Latcham, A. M. Grimes, D. P. Hurp, K. M. Downham, G. J. Sanger, W. J. Winchester, A. D. Morrison, and G. B. Moore. 2009. 'UDP-glucose modulates gastric function through P2Y14 receptor-dependent and -independent mechanisms', *Am J Physiol Gastrointest Liver Physiol*, 296: G923-30.
Budnick, J. A., X. R. Bina, and J. E. Bina. 2021. 'Complete Genome Sequence of Klebsiella pneumoniae Strain ATCC 43816', *Microbiol Resour Announc*, 10.
Cliffe, E. E., and S. G. Waley. 1961. 'The mechanism of the glyoxalase I reaction, and the effect of ophthalmic acid as an inhibitor', *Biochem J*, 79: 475-82.
Colosimo, D. A., J. A. Kohn, P. M. Luo, F. J. Piscotta, S. M. Han, A. J. Pickard, A. Rao, J. R. Cross, L. J. Cohen, and S. F. Brady. 2019. 'Mapping Interactions of

1331 Microbial Metabolites with Human G-Protein-Coupled Receptors', *Cell Host*
1332 *Microbe*, 26: 273-82.e7.
1333 Darfeuille-Michaud, A., C. Neut, N. Barnich, E. Lederman, P. Di Martino, P.
1334 Desreumaux, L. Gambiez, B. Joly, A. Cortot, and J. F. Colombel. 1998.
1335 'Presence of adherent Escherichia coli strains in ileal mucosa of patients with
1336 Crohn's disease', *Gastroenterology*, 115: 1405-13.
1337 Darveau, R. P., J. Blake, C. L. Seachord, W. L. Cosand, M. D. Cunningham, L.
1338 Cassiano-Clough, and G. Maloney. 1992. 'Peptides related to the carboxyl
1339 terminus of human platelet factor IV with antibacterial activity', *The Journal of*
1340 *Clinical Investigation*, 90: 447-55.
1341 Datsenko, K. A., and B. L. Wanner. 2000. 'One-step inactivation of chromosomal
1342 genes in Escherichia coli K-12 using PCR products', *Proc Natl Acad Sci USA*,
1343 97.
1344 Di Stasi, L. C. 2021. 'Coumarin Derivatives in Inflammatory Bowel Disease',
1345 *Molecules*, 26.
1346 Faas, M. M., T. Saez, and P. de Vos. 2017. 'Extracellular ATP and adenosine: The
1347 Yin and Yang in immune responses?', *Mol Aspects Med*.
1348 Falla, T. J., D. N. Karunaratne, and R. E. Hancock. 1996. 'Mode of action of the
1349 antimicrobial peptide indolicidin', *J Biol Chem*, 271: 19298-303.
1350 Garavaglia, M., E. Rossi, and P. Landini. 2012. 'The pyrimidine nucleotide biosynthetic
1351 pathway modulates production of biofilm determinants in Escherichia coli',
1352 *PLOS ONE*, 7: e31252.
1353 Gobbo, M., M. Benincasa, G. Bertoloni, B. Biondi, R. Dosselli, E. Papini, E. Reddi, R.
1354 Rocchi, R. Tavano, and R. Gennaro. 2009. 'Substitution of the arginine/leucine
1355 residues in apidaecin Ib with peptoid residues: effect on antimicrobial activity,
1356 cellular uptake, and proteolytic degradation', *J Med Chem*, 52: 5197-206.
1357 Hale, T. L., E. V. Oaks, and S. B. Formal. 1985. 'Identification and antigenic
1358 characterization of virulence-associated, plasmid-coded proteins of Shigella
1359 spp. and enteroinvasive Escherichia coli', *Infect Immun*, 50: 620-9.
1360 Kim, E. K., K. A. Lee, D. Y. Hyeon, M. Kyung, K. Y. Jun, S. H. Seo, D. Hwang, Y.
1361 Kwon, and W. J. Lee. 2020. 'Bacterial Nucleoside Catabolism Controls Quorum
1362 Sensing and Commensal-to-Pathogen Transition in the Drosophila Gut', *Cell*
1363 *Host Microbe*.
1364 Larrick, J. W., M. Hirata, Y. Shimomoura, M. Yoshida, H. Zheng, J. Zhong, and S. C.
1365 Wright. 1993. 'Antimicrobial activity of rabbit CAP18-derived peptides',
1366 *Antimicrobial Agents and Chemotherapy*, 37: 2534-9.
1367 Lee, S. B., B. Li, S. Jin, and H. Daniell. 2011. 'Expression and characterization of
1368 antimicrobial peptides Retrocyclin-101 and Protegrin-1 in chloroplasts to control
1369 viral and bacterial infections', *Plant Biotechnol J*, 9: 100-15.
1370 Liu, C., Y. Cheng, Y. Guo, and H. Qian. 2021. 'Magnesium-L-threonate alleviate
1371 colonic inflammation and memory impairment in chronic-plus-binge alcohol
1372 feeding mice', *Brain Res Bull*, 174: 184-93.
1373 Luchini, A. C., P. Rodrigues-Orsi, S. H. Cestari, L. N. Seito, A. Witaicenis, C. H.
1374 Pellizzon, and L. C. Di Stasi. 2008. 'Intestinal anti-inflammatory activity of
1375 coumarin and 4-hydroxycoumarin in the trinitrobenzenesulphonic acid model of
1376 rat colitis', *Biol Pharm Bull*, 31: 1343-50.
1377 O'Donnell, M. P., B. W. Fox, P. H. Chao, F. C. Schroeder, and P. Sengupta. 2020. 'A
1378 neurotransmitter produced by gut bacteria modulates host sensory behaviour',
1379 *Nature*, 583: 415-20.

Offord, R. E., J. Philippe, J. G. Davis, P. A. Halban, and M. Berger. 1979. 'Inhibition of degradation of insulin by ophthalamic acid and by a bovine pancreatic proteinase inhibitor', *Biochem J*, 182: 249-51.

Ohsu, T., Y. Amino, H. Nagasaki, T. Yamanaka, S. Takeshita, T. Hatanaka, Y. Maruyama, N. Miyamura, and Y. Eto. 2010. 'Involvement of the calcium-sensing receptor in human taste perception', *J Biol Chem*, 285: 1016-22.

Selsted, M. E., M. J. Novotny, W. L. Morris, Y. Q. Tang, W. Smith, and J. S. Cullor. 1992. 'Indolicidin, a novel bactericidal tridecapeptide amide from neutrophils', *J Biol Chem*, 267: 4292-5.

Soga, T., R. Baran, M. Suematsu, Y. Ueno, S. Ikeda, T. Sakurakawa, Y. Kakazu, T. Ishikawa, M. Robert, T. Nishioka, and M. Tomita. 2006. 'Differential metabolomics reveals ophthalmic acid as an oxidative stress biomarker indicating hepatic glutathione consumption', *J Biol Chem*, 281: 16768-76.

Sridharan, G. V., K. Choi, C. Klemashevich, C. Wu, D. Prabakaran, L. B. Pan, S. Steinmeyer, C. Mueller, M. Yousofshahi, R. C. Alaniz, K. Lee, and A. Jayaraman. 2014. 'Prediction and quantification of bioactive microbiota metabolites in the mouse gut', *Nat Commun*, 5: 5492.

Steiner, M. R., J. S. Bomalaski, and M. A. Clark. 1993. 'Responses of purified phospholipases A2 to phospholipase A2 activating protein (PLAP) and melittin', *Biochim Biophys Acta*, 1166: 124-30.

Sun, Q., J. G. Weinger, F. Mao, and G. Liu. 2016. 'Regulation of structural and functional synapse density by L-threonate through modulation of intraneuronal magnesium concentration', *Neuropharmacology*, 108: 426-39.

Wang, J., K. Ma, M. Ruan, Y. Wang, Y. Li, Y. V. Fu, Y. Song, H. Sun, and J. Wang. 2018. 'A novel cecropin B-derived peptide with antibacterial and potential anti-inflammatory properties', *PeerJ*, 6: e5369.

Zaslaver, A., A. Bren, M. Ronen, S. Itzkovitz, I. Kikoin, S. Shavit, W. Liebermeister, M. G. Surette, and U. Alon. 2006. 'A comprehensive library of fluorescent transcriptional reporters for Escherichia coli', *Nat Methods*, 3: 623-8.

Fig. 1 eATP triggers a strong transcriptomic response in *E. coli* in a medium-, dose- and time-dependent manner

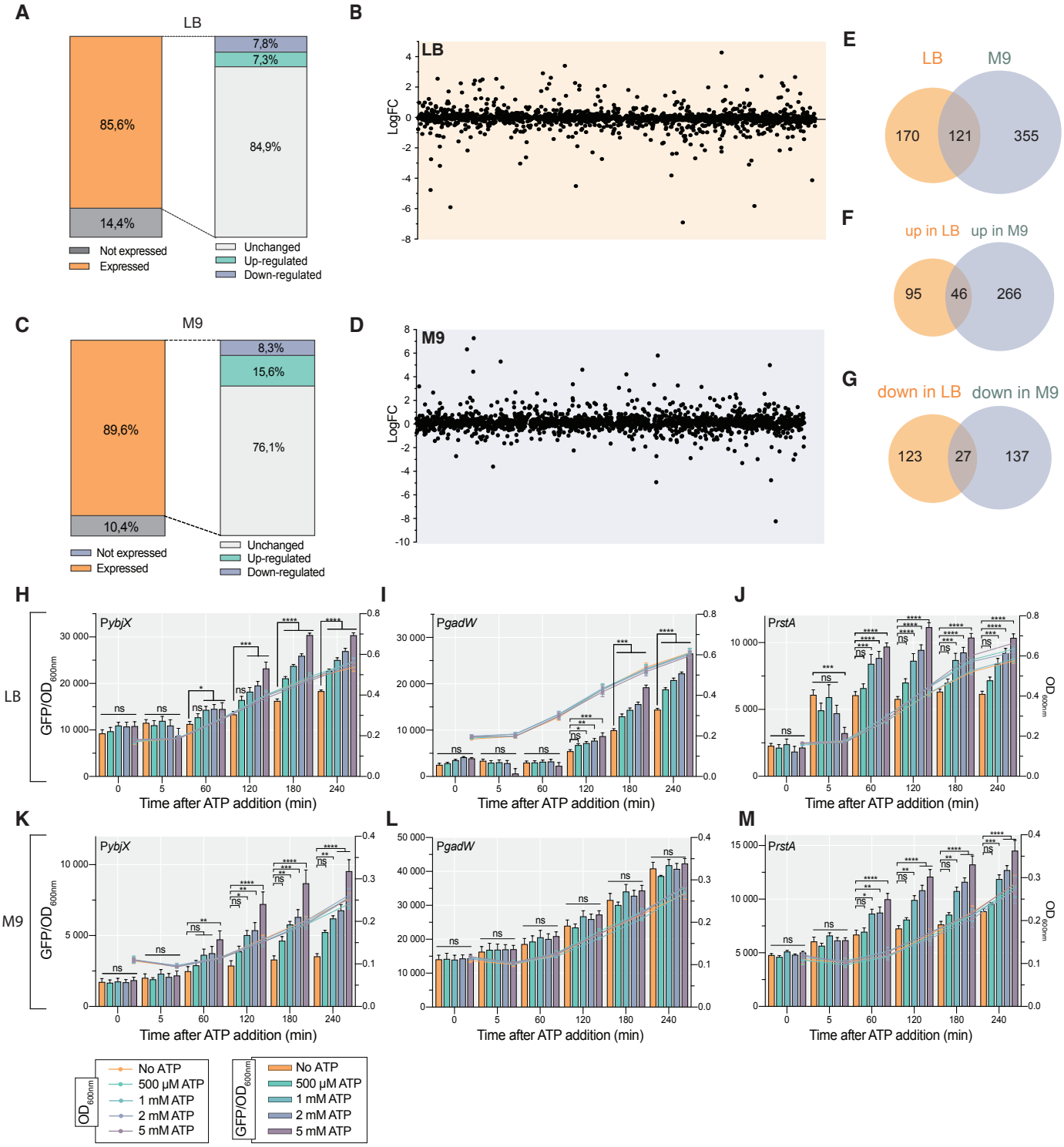

Fig. 2 eATP modulates genes involved in critical pahtways, such as lipids, amino acid or vitamin metabolism

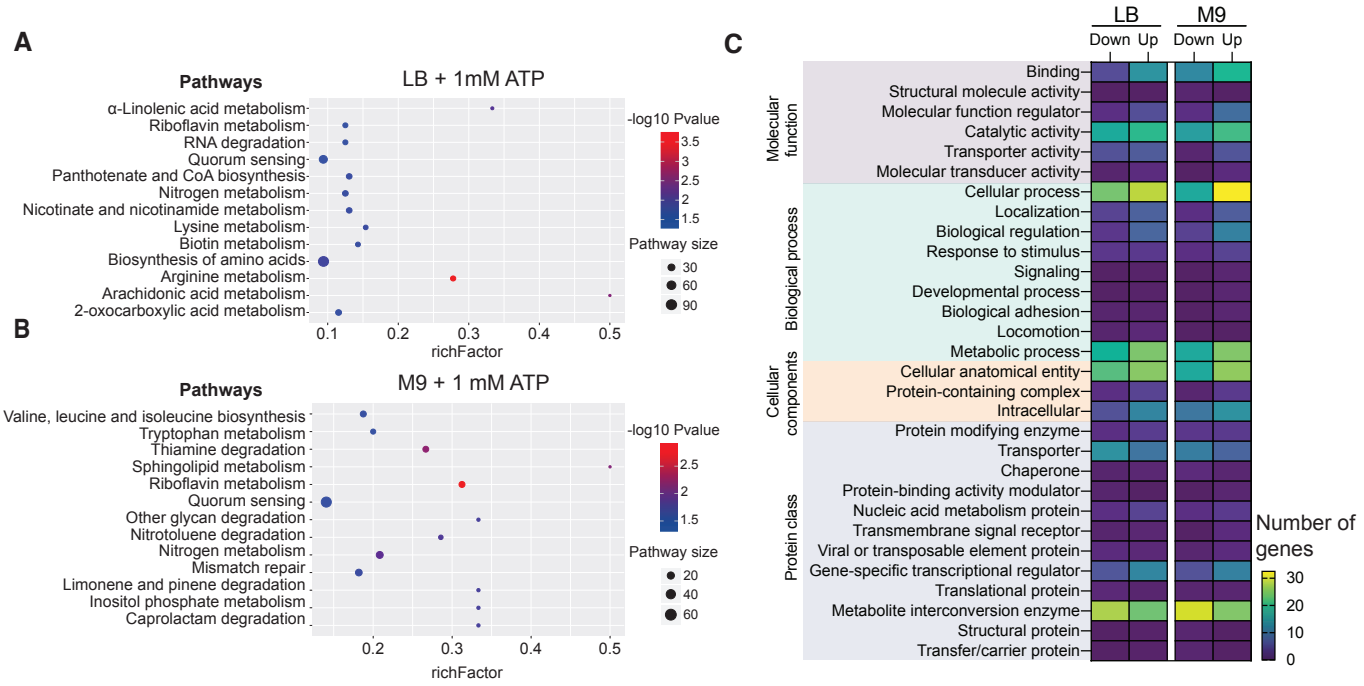

Fig. 3 Intracellular metabolites quantification upon exposure to eATP

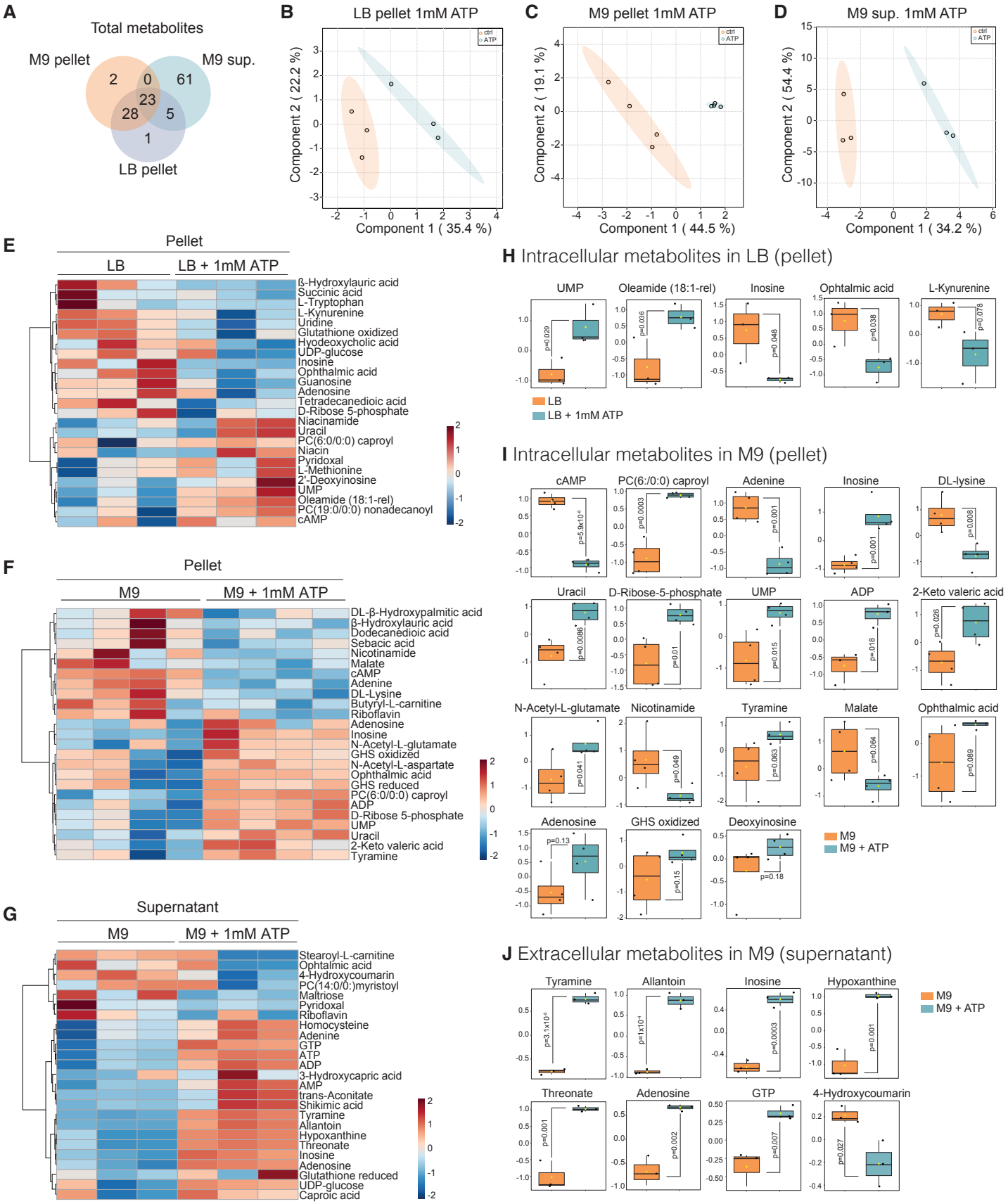

Fig. 4.Reaction fluxes enrichment analysis and biomass building blocks analysis

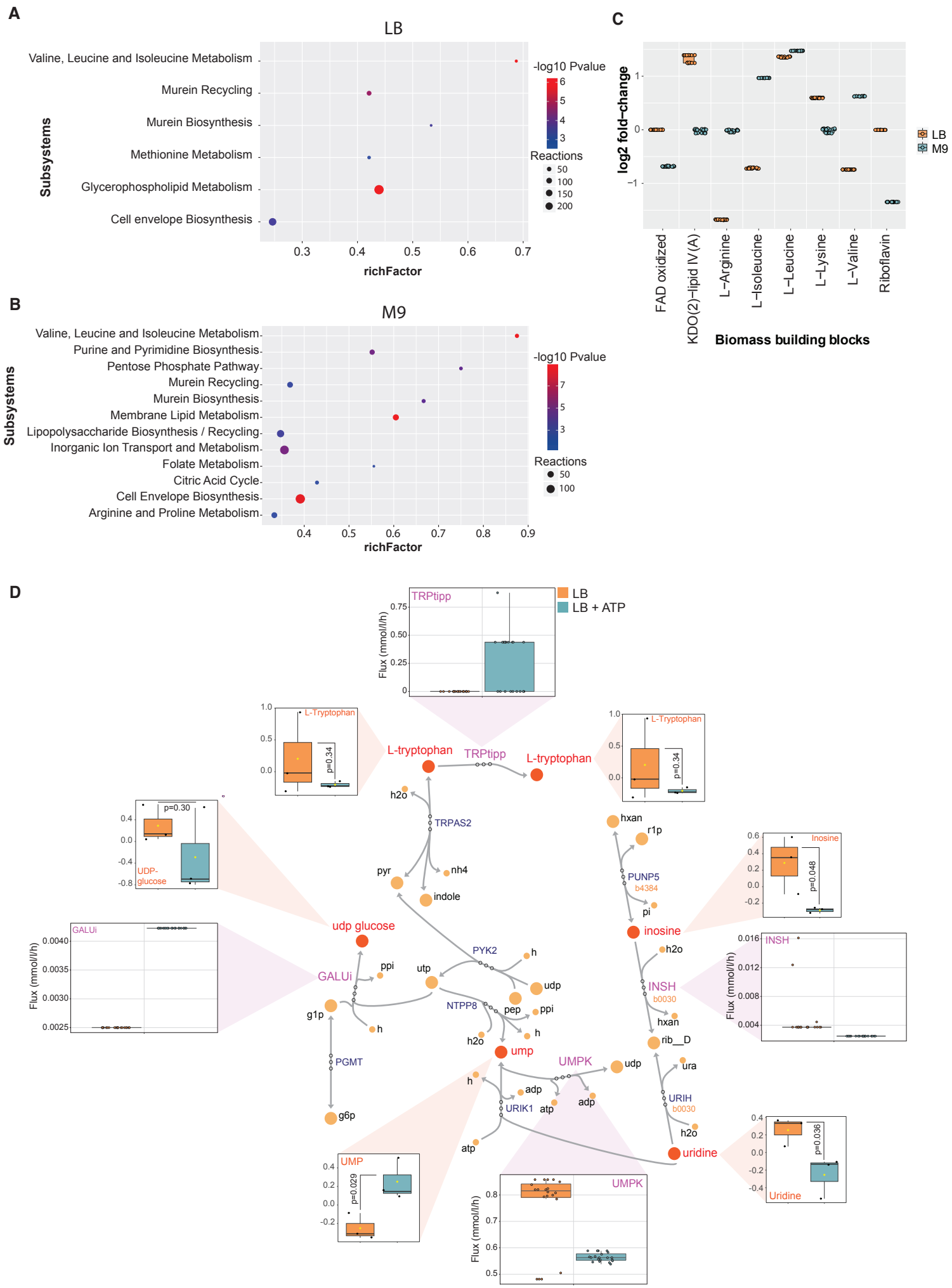

Fig. 5 Metabolic map of eATP impact in LB

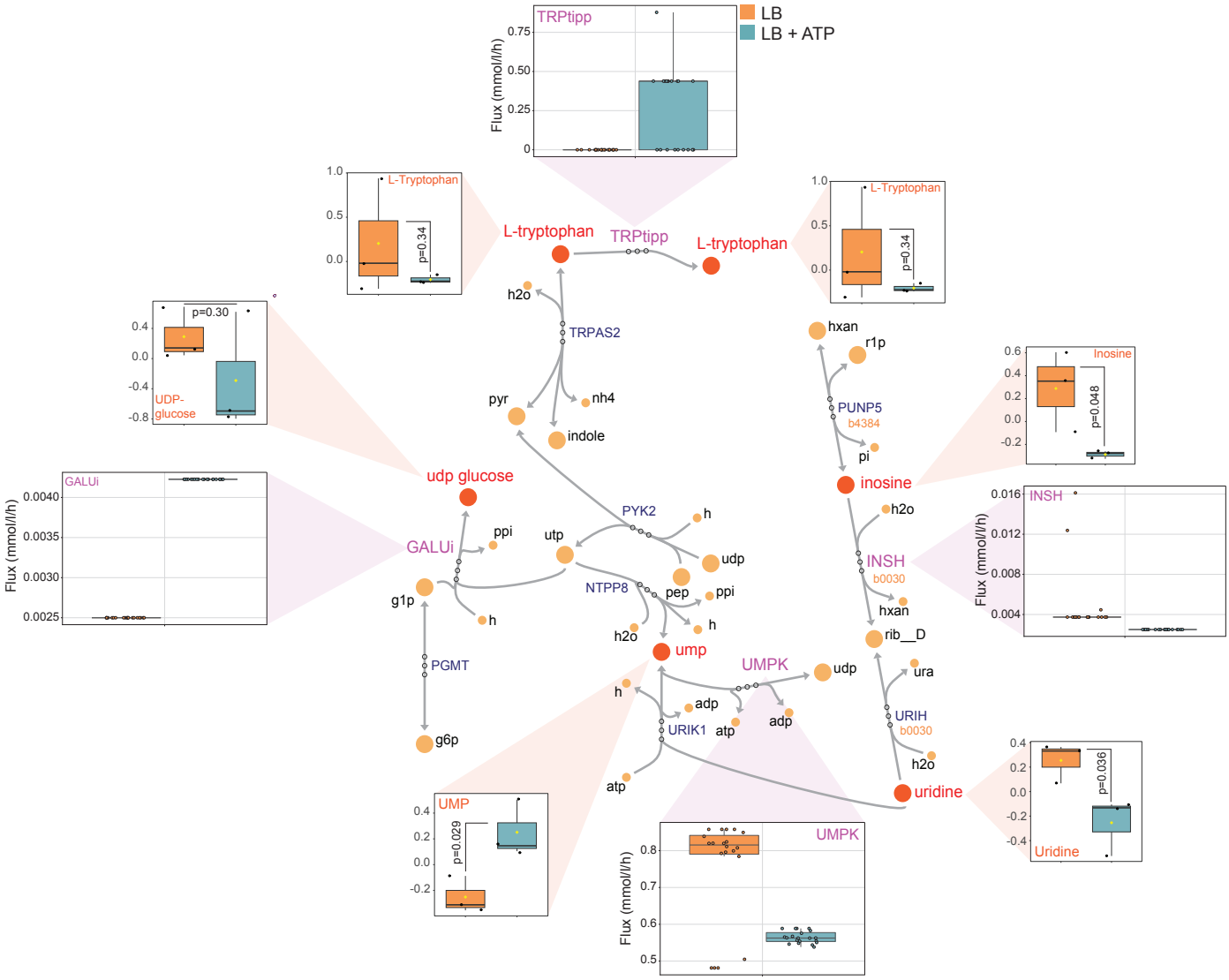

Fig. 6 Antimicrobial molecule susceptibility and response to eATP in other bacteria

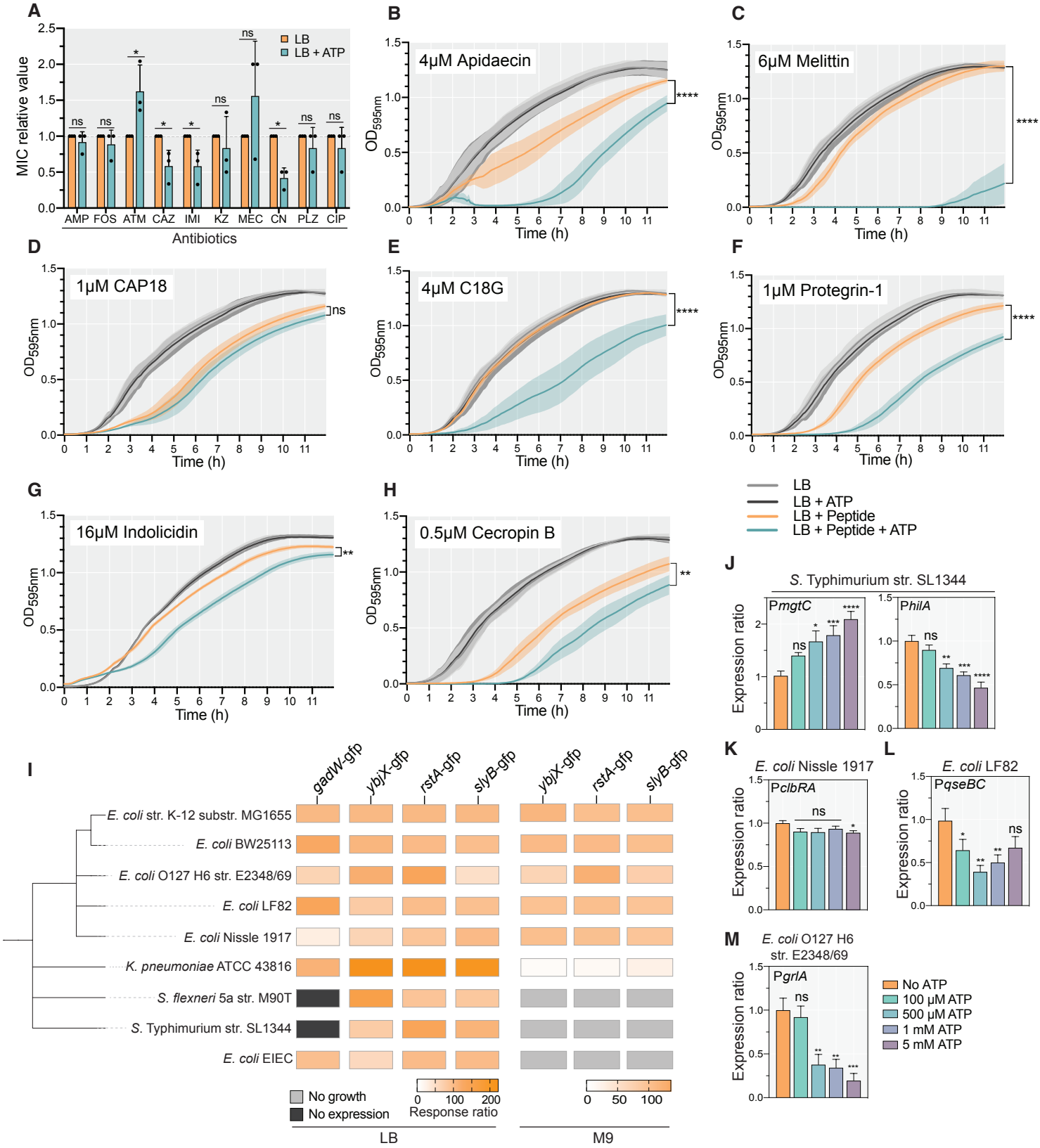

Fig. EV1 Promoter library screening, figure related to Fig. 1

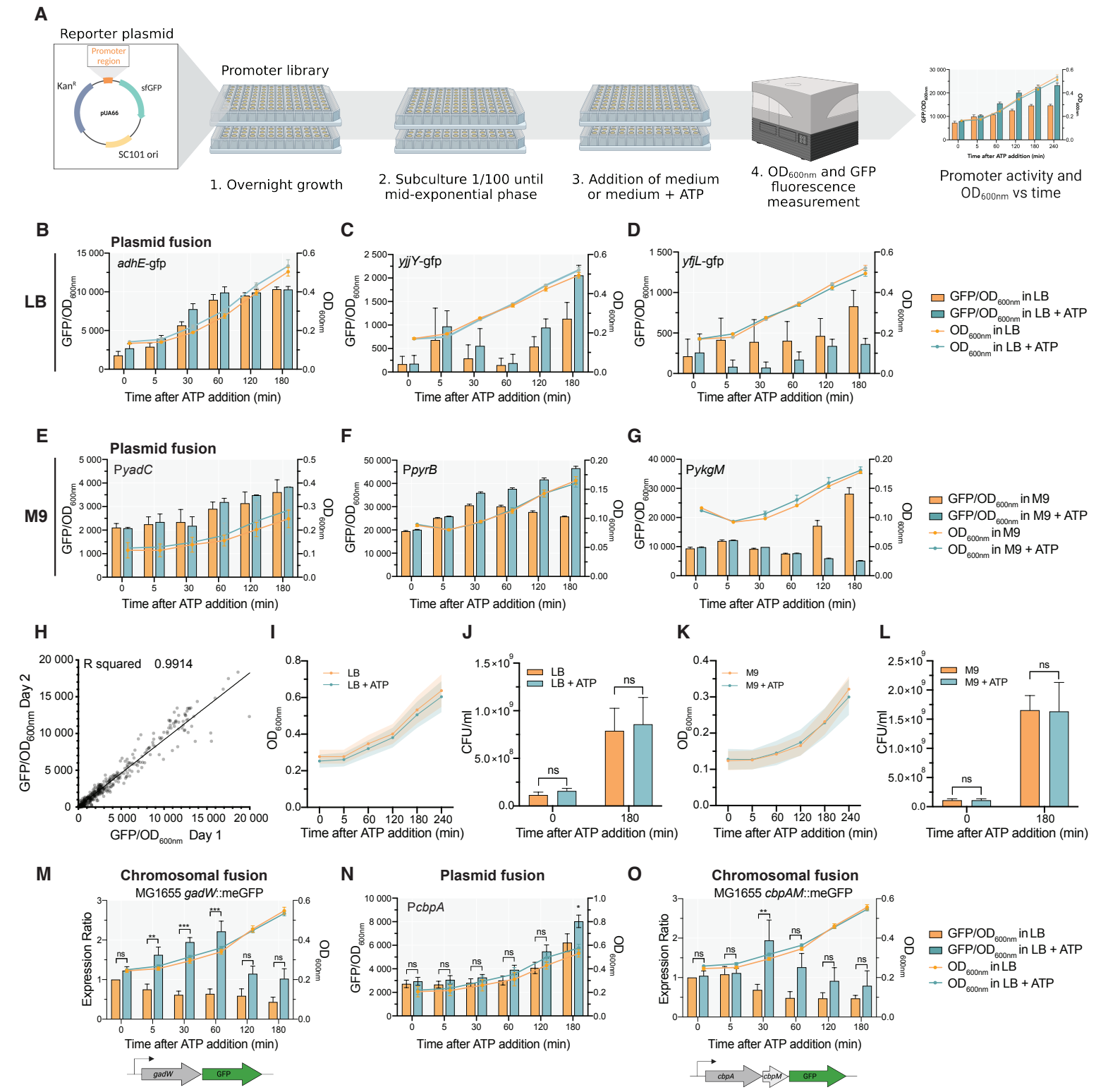

Fig. EV2 Intracellular metabolites quantification upon exposure to 1mM ATP in LB and M9

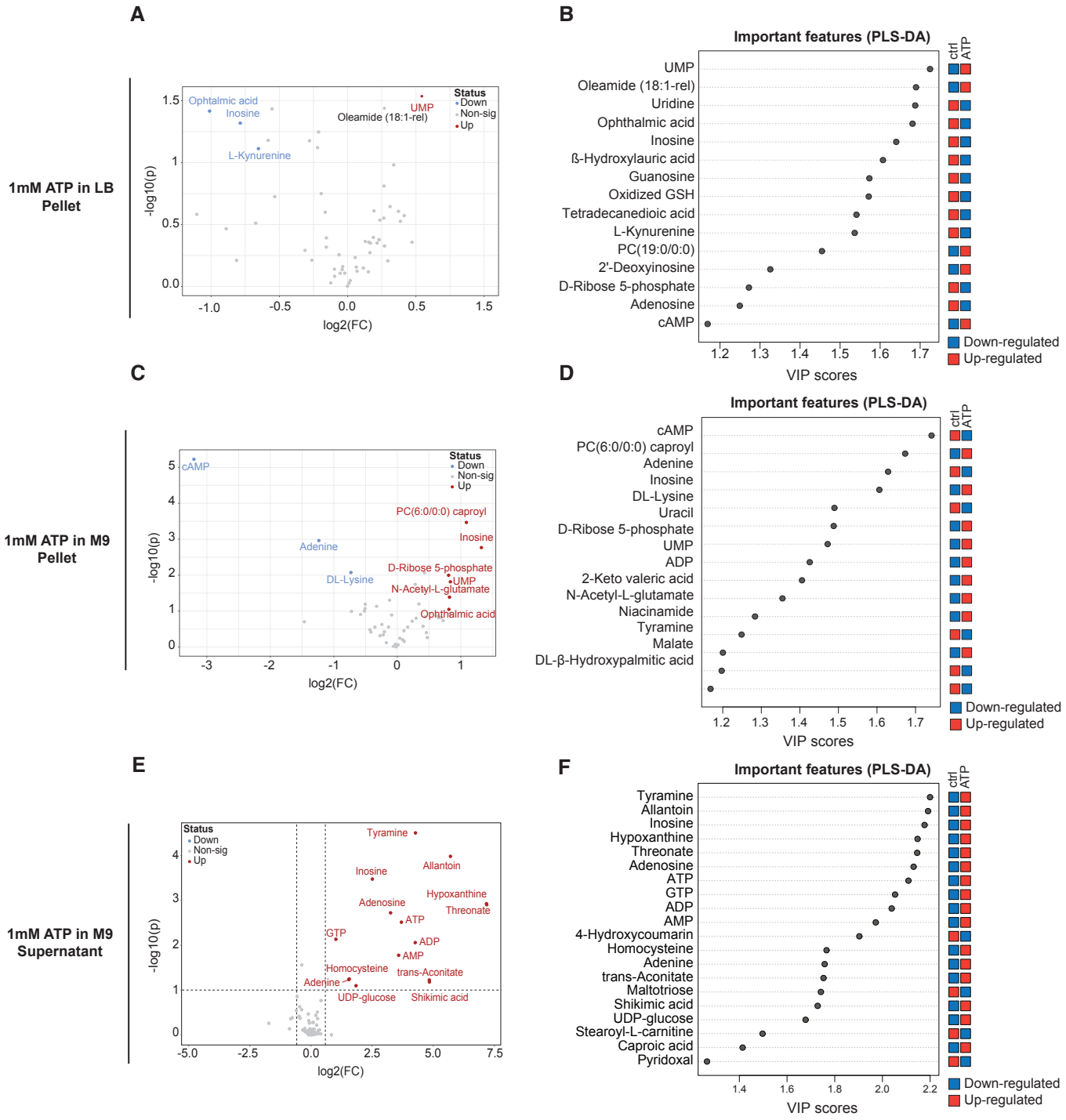

Fig.EV3 Intracellular metabolites modulation upon exposure to 100 μM ATP in M9

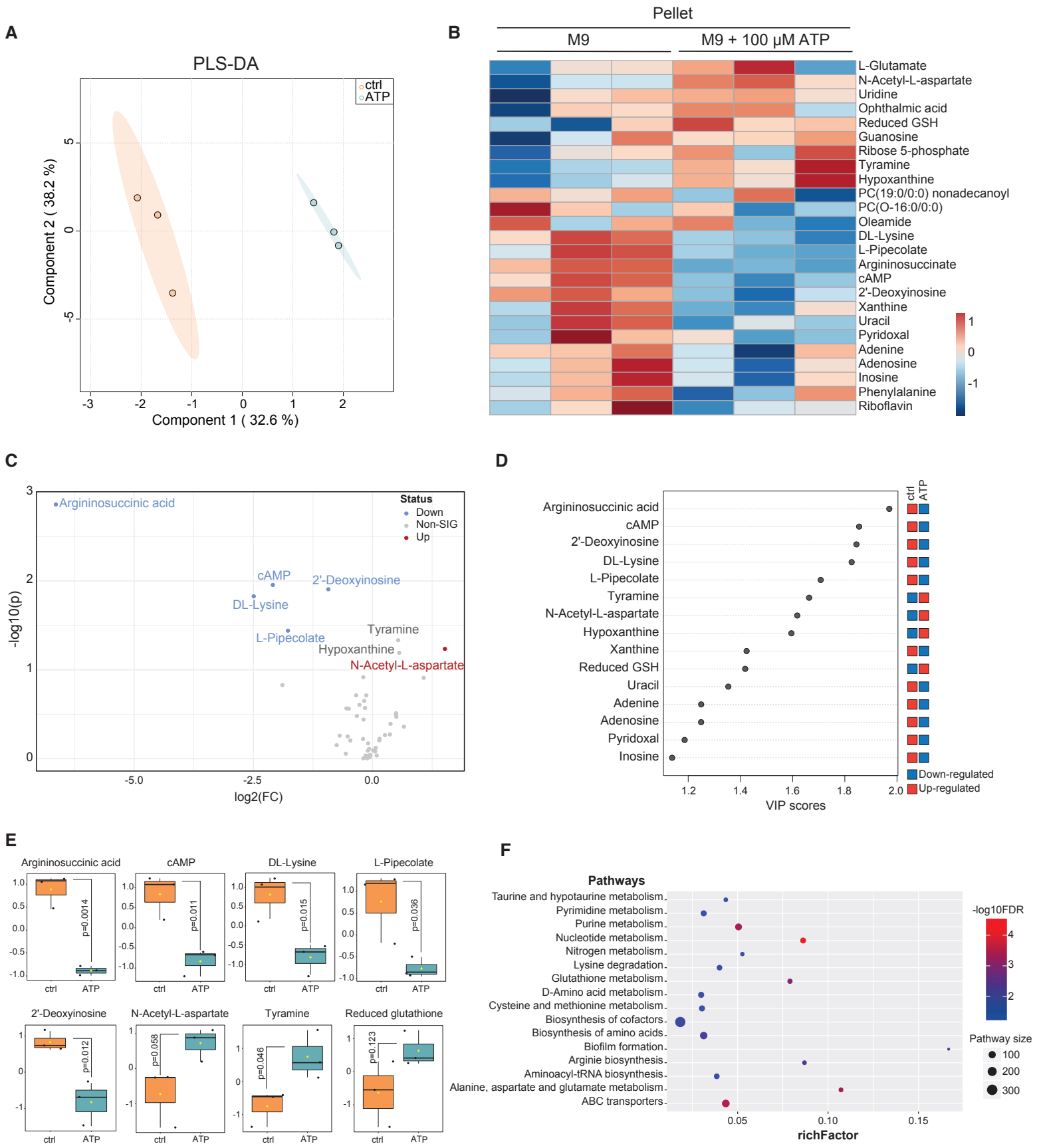

Fig.EV4 AMP susceptibility

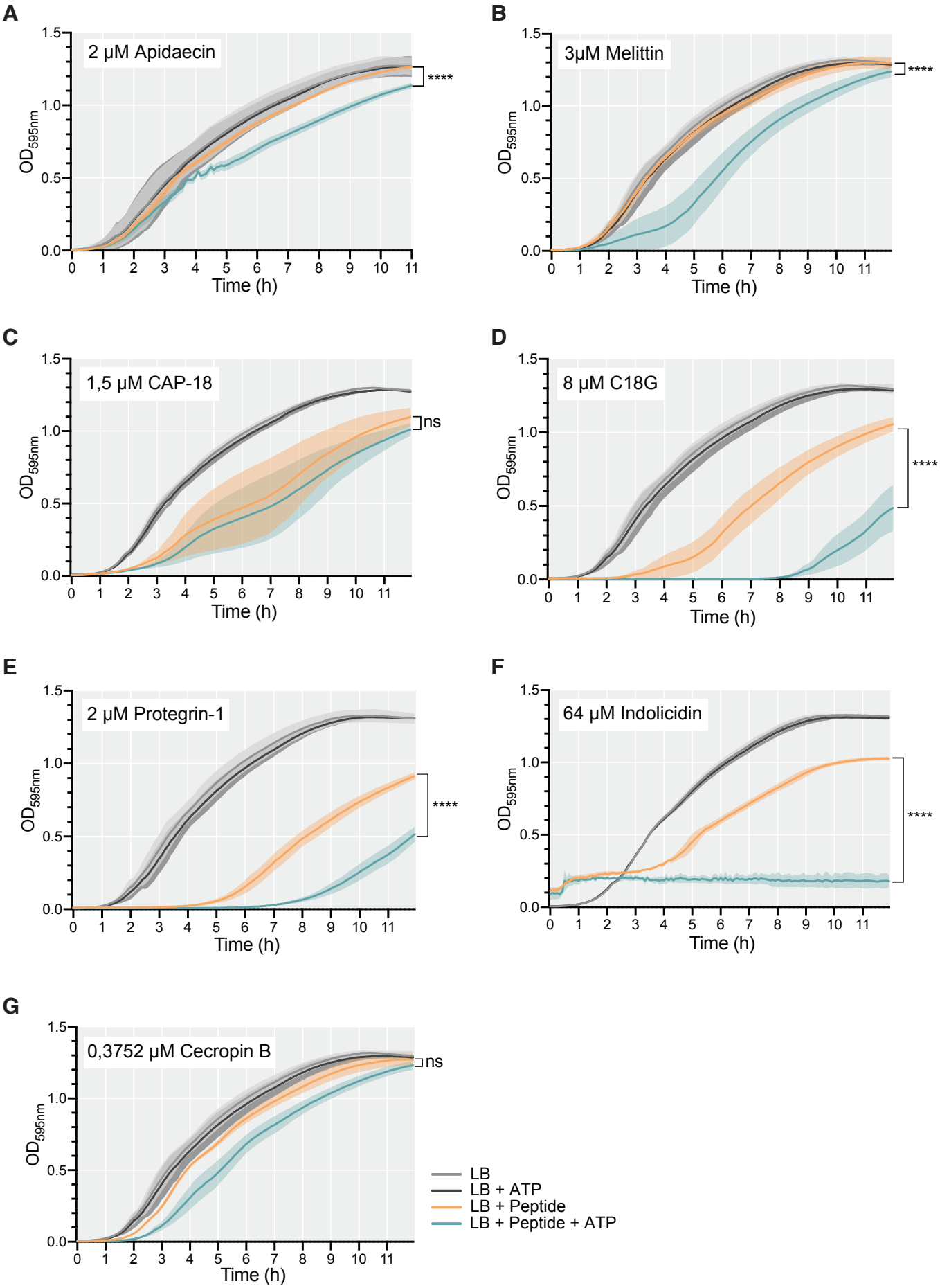
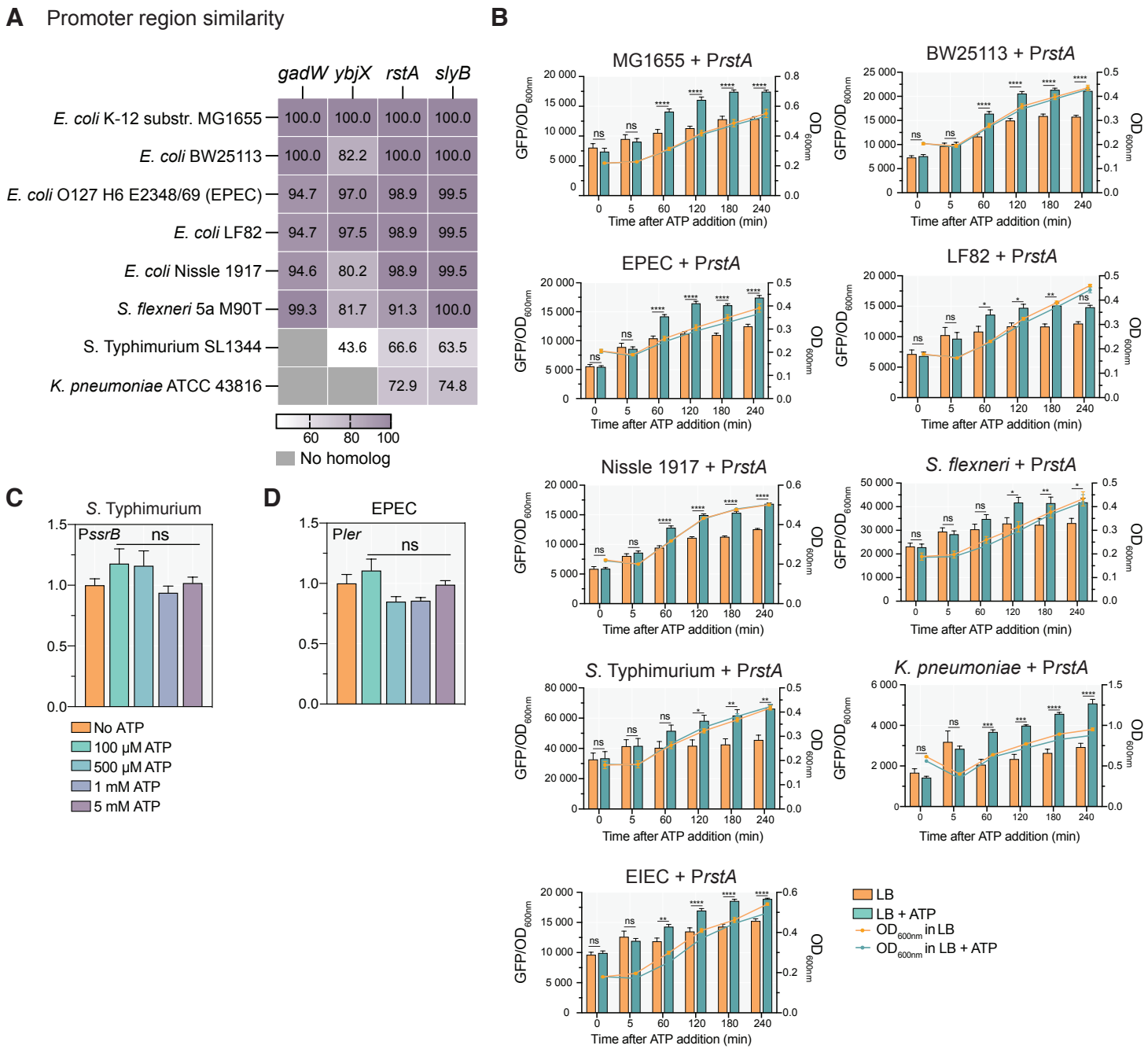
Fig. EV5 - eATP triggers a transcriptional response in several bacteria and regulates the expression of virulence factors.